HOKKAIDO UNIVERSITY

Title	Dopamine regulates astrocytic IL-6 expression and process formation via dopamine receptors and adrenoceptors
Author(s)	Morimoto, Kohei; Ouchi, Mai; Kitano, Taisuke et al.
Citation	European journal of pharmacology, 928, 175110 https://doi.org/10.1016/j.ejphar.2022.175110
Issue Date	2022-08-05
Doc URL	https://hdl.handle.net/2115/90384
Rights	© <2022>. This manuscript version is made available under the CC-BY-NC-ND 4.0 license http://creativecommons.org/licenses/by-nc-nd/4.0/
Rights(URL)	https://creativecommons.org/licenses/by-nc-nd/4.0/
Type	journal article
File Information	Manuscript.pdf

Hokkaido University Collection of Scholarly and Academic Papers : HUSCAP

Title

Dopamine regulates astrocytic IL-6 expression and process formation via dopamine receptors and adrenoceptors

The full names of the authors

Kohei Morimoto, Mai Ouchi, Taisuke Kitano, Ryota Eguchi, and Ken-ichi Otsuguro

Corresponding author: Ken-ichi Otsuguro

Laboratory of Pharmacology, Department of Basic Veterinary Sciences, Faculty of Veterinary Medicine, Hokkaido University, Kita 18, Nishi 9, Kita-ku, Sapporo 060-0818, Japan. Tel/Fax: +81-11-706-5220; E-mail: otsuguro@vetmed.hokudai.ac.jp

The author's institutional affiliations

Laboratory of Pharmacology, Department of Basic Veterinary Sciences, Faculty of Veterinary Medicine, Hokkaido University, Kita 18, Nishi 9, Kita-ku, Sapporo 060-0818, Japan.

Abstract

Dopamine levels in the central nervous system change under pathological conditions such as Parkinson's disease, Huntington's disease, and addiction. Under those pathological conditions, astrocytes become reactive astrocytes characterized by morphological changes and the release of inflammatory cytokines involved in pathogenesis. However, it remains unclear whether dopamine regulates astrocytic morphology and functions. Elucidating these issues will help us to understand the pathogenesis of neurodegenerative diseases caused by abnormal dopamine signaling. In this study, we investigated the effects of dopamine on IL-6 expression and process formation in rat primary cultured astrocytes and acute hippocampal slices. Dopamine increased IL-6 expression in a concentration-dependent manner, and this was accompanied by CREB phosphorylation. The effects of a low dopamine concentration (1 μM) were inhibited by a D1-like receptor antagonist, whereas the effects of a high dopamine concentration (100 μM) were inhibited by a ß-antagonist and enhanced by a D2-like receptor antagonist. Furthermore, dopamine (100 μM) promoted process formation, which was inhibited by a ß-antagonist and enhanced by both an α-antagonist and a D2-like receptor antagonist. In acute hippocampal slices, both a D1-like receptor agonist and ß-agonist changed astrocytic morphology. Together, these results indicate that dopamine promotes IL-6 expression and process formation via D1-like receptors and ß-adrenoceptors. Furthermore, bidirectional

regulation exists; namely, the effects of D1-like receptors and β-adrenoceptors were negatively regulated by D2-like receptors and α_2-adrenoceptors.

Keywords

astrocyte, dopamine, adrenoceptor, IL-6, CREB, morphology

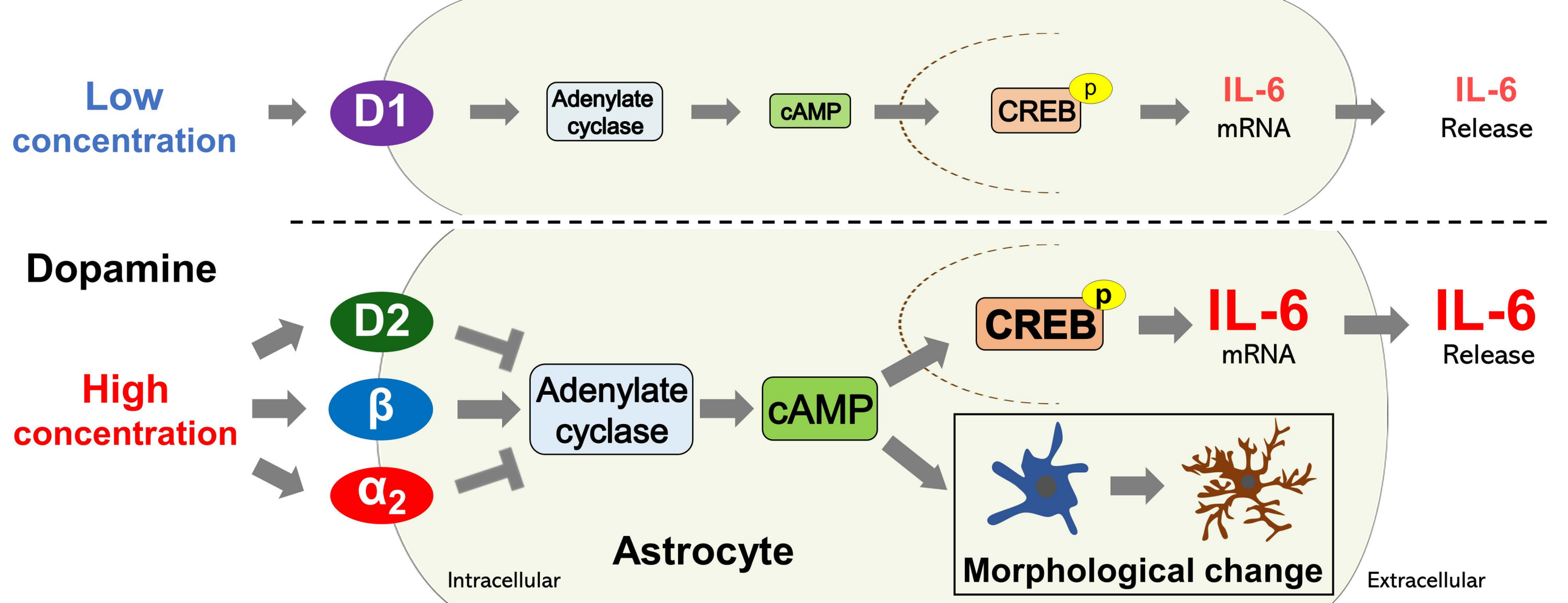
Low
concentration
D1
Adenylate
cyclase
cAMP
CREB
p
IL-6
mRNA
IL-6
Release
Dopamine
High
concentration
D2
β
α2
Adenylate
cyclase
cAMP
CREB
p
IL-6
mRNA
IL-6
Release
Morphological change
Astrocyte
Intracellular
Extracellular

1. Introduction

Dopamine is a key neurotransmitter in the central nervous system (CNS) and regulates many brain functions (Klein et al., 2019). Dopaminergic neurons project to most regions of the CNS, including the cerebral cortex, hippocampus, and spinal cord (Descarries et al., 1987; Edelmann and Lessmann, 2018; Ridet et al., 1992). Dopamine is released not only from synapses but also from varicosities (Fuxe et al., 2015), and thus acts on astrocytes, a type of glial cell that surrounds neurons. Astrocytic cytokine production and the morphology of astrocytic processes are closely related to the physiological functions of the CNS. In the CNS, astrocytes represent the major source of interleukin-6 (IL-6) (Gruol and Nelson, 1997), which suppresses neuronal cell death (Day et al., 2014) and acts as a neurotrophic factor (Wagner, 1996). Astrocytic processes contact neurons, forming the "tripartite synapse" that regulates synaptic function (Allen and Eroglu, 2017).

Dopamine levels in the CNS change under pathological conditions such as Parkinson's disease, Huntington's disease, and addiction (Klein et al., 2019). Furthermore, astrocytes transform into reactive astrocytes in response to a wide range of neurodegenerative diseases (Hart and Karimi-Abdolrezaee, 2021; Pekny and Nilsson, 2005). Reactive astrocytes are characterized by upregulated IL-6 and glial fibrillary acidic protein (GFAP) expression and distinct morphological changes (Escartin et al., 2021; John

et al., 2003; Sofroniew, 2009), and regarded as reflections of a detrimental astrocyte phenotype, which contribute to various pathogeneses (Escartin et al., 2021). Chronic IL-6 overexpression in astrocytes induces an inflammatory response (Penkowa et al., 2003). Impaired astrocytic morphogenesis links to diminished function of excitatory synapses (Stogsdill et al., 2017), and astrocytic morphology regulates scar formation, facilitating recovery from traumatic brain injury (Schiweck et al., 2021). Furthermore, the activation of astrocytic dopamine receptors regulates neuroinflammation (Montoya et al., 2019; Zhu et al., 2018) and depresses excitatory synaptic transmission (Corkrum et al., 2020). These reports suggest that dopamine is involved in the pathogenesis of CNS diseases via its action on astrocytes.

Astrocytes express D1-like receptors (D1, D5), D2-like receptors (D2-D4) (Miyazaki et al., 2004), α_1-, α_2-, and ß-adrenoceptors (Hertz et al., 2010). Dopamine has a low affinity for adrenoceptors (Zhang et al., 2004). High dopamine concentrations act on ß-adrenoceptors in astrocytes, activating brain-derived neurotrophic factor (BDNF) transcription and changing cell morphology (Koppel et al., 2018). Our previous reports have demonstrated that noradrenaline acts on astrocytic ß-adrenoceptors to enhance IL-6 transcription and change cell morphology (Kitano et al., 2021; Morimoto et al., 2021). However, it remains unknown whether dopamine affects astrocytic IL-6 production or morphology and, if so, which receptors are involved. Such knowledge could enhance our

82 understanding of the role that dopamine plays in astrocytic functions and the
83 pathogenesis of neurodegenerative diseases caused by abnormal dopamine signaling. We
84 aimed to comprehensively identify IL-6 expression and morphological changes as a
85 phenotype of reactive astrocytes.

86 In this study, we investigated dopamine-induced IL-6 expression and
87 morphological changes in rat cultured astrocytes and acute brain slices. The results
88 revealed the concentration-dependent effects of dopamine acting via dopamine and
89 adrenergic receptors and its intracellular mechanisms.

90

2. Materials and Methods

2.1. Materials

Antibodies against the following were used: ERK 1/2 (extracellular signal-regulated kinase 1/2) (#4695S, 1:2500), phospho-ERK 1/2 (#9101S, 1:2500), p38 (#9212S, 1:2000), phospho-p38 (#9211S, 1:1000), SAPK/JNK (c-jun N-terminal kinase) (#9252S, 1:2500), phospho-SAPK/JNK (#9251S, 1:1500), STAT3 (Signal transducer and activator of transcription 3) (#4904S, 1:4000), and phospho-STAT3 (#9145S, 1:2000) (all from Cell Signaling Technology, Danvers, MA, USA); CREB (cAMP response element-binding protein) (#sc-377154, 1:500) and phospho-CREB (#sc-81486, 1:250) (both from Santa Cruz Biotechnology, Santa Cruz, CA, USA); and GFAP (#11051, 1:200, Immuno-Biological Laboratories, Gunma, Japan).

The following reagents were used: atenolol, atipamezole hydrochloride, 2-bromo-α-ergocryptine methanesulfonate salt (bromocriptine), and isoproterenol hydrochloride (all from Sigma-Aldrich, St. Louis, MO, USA); propranolol hydrochloride, forskolin, histamine dihydrochloride, and L(+)-ascorbic acid (all from FUJIFILM Wako Pure Chemical, Osaka, Japan); 1-phenyl-2,3,4,5-tetrahydro-1H-3-benzazepine hydrochloride (SCH23390), (±)-6-chloro-2,3,4,5-tetrahydro-1-phenyl-1H-3-benzazepine hydrobromide (SKF81297), 6-chloro-2,3,4,5-tetrahydro-1-(3-methylphenyl)-3-(2-propenyl)-1H-3-

benzazepine-7,8-diol hydrobromide (SKF83822), and 6-chloro-2,3,4,5-tetrahydro-3-methyl-1-(3-methylphenyl)-1H-3-benzazepine-7,8-diol (SKF83959) (all from Tocris Bioscience, Bristol, UK); ICI118551 hydrochloride and SR59230A (both from MedChemExpress, Monmouth Junction, NJ, USA); 3-hydroxytyramine hydrochloride (dopamine; Tokyo Chemical Industry, Tokyo, Japan); haloperidol (Pfizer, New York, NY, USA); and 5-hydroxytryptamine hydrochloride (5-HT; Nacalai Tesque, Kyoto, Japan).

2.2. Animals

All animal care and experimental protocols were approved by the Committee on Animal Experimentation, Graduate School of Veterinary Medicine, Hokkaido University (No. 19-0009), which was awarded the Accreditation Status by the Association for Assessment and Accreditation of Laboratory Animal Care International. Animal studies were performed in compliance with ARRIVE guidelines (Percie du Sert et al., 2020). Wistar rats were obtained from CLEA Japan (Tokyo, Japan) and were bred to obtain pups. The rats were fed *ad libitum* and kept on a 12 h light-dark cycle at 22 ± 4 °C. Male and female pups (3-5 days old) were used for primary astrocyte cultures, and male pups (14-16 days old) were used for acute brain slice experiments.

2.3. Primary cultured astrocytes

Primary cultured astrocytes were obtained as previously described (Morimoto et al., 2020). In brief, the cerebral cortex, hippocampus, and spinal cords were isolated from rat pups (3-5 days old), minced, and incubated with papain (10 U/ml) and DNase (0.1 mg/ml). Dissociated cells were suspended in Dulbecco's modified Eagle's medium/Ham's F-12 (#048-29785, FUJIFILM Wako Pure Chemical) containing 10% fetal bovine serum, 100 U/ml penicillin, and 0.1 mg/ml streptomycin. The cell suspension was seeded onto a poly-l-lysine-coated T75 flask. After 7-8 days, the flask was shaken at 250 rpm at 37 °C for at least 12 h to remove all cells except astrocytes. Adherent cells were detached with trypsin and re-seeded onto poly-l-lysine-coated 12-well plates or coverslips at a density of 8.0×10^3 cells/cm^2. After 3 days, the cell culture reached confluence, and the medium was changed to serum-free medium. Cell cultures were first treated with antagonists immediately after the medium exchange and were then treated with dopamine or other agonists 1 h after the medium exchange. After a certain amount of time (detailed in the figure legends and results section), the cell culture was used for experiments. The concentrations of dopamine used in this study were determined based on the previous reports (Cragg and Rice, 2004; Koppel et al., 2018). Agonists and antagonists were used at concentrations specific to the target receptors, based on the database ("IUPHAR / BPS Guide to PHARMACOLOGY" https://www.guidetopharmac). The purity of astrocyte

147 cultures was evaluated by immunostaining for the astrocytic marker GFAP. At least 300
148 cells in 12 randomly selected images from three cultures (cerebral cortex, hippocampus,
149 and spinal cord) were evaluated, and all cells we evaluated were positive for GFAP (Fig.
150 S1 and Kitano et al., 2021).
151
152 **2.4. RNA extraction and real-time PCR analyses**
153 Total RNA was extracted from cultured astrocytes using RNAiso Plus (Takara Bio,
154 Tokyo, Japan). To remove genomic DNA and synthesize cDNA, the RNA sample was then
155 incubated with qPCR RT Master Mix with gDNA Remover (TOYOBO, Osaka, Japan).
156 Real-time PCR was performed using Thunderbird SYBR qPCR Mix (TOYOBO), each
157 primer, and the cDNA reaction solution. The primer sequences are provided in Table S1.
158 Thermal cycles were performed using the Eco Real-Time PCR System (Illumina, San Diego,
159 CA, USA). Cycling conditions were 95 °C for 1 min (for initial denaturation), followed by
160 40 cycles of denaturation (95 °C, 15 s), annealing, and extension (temperature: Table S1,
161 45 s). RNAs without reverse transcription were used as a negative control to examine DNA
162 contamination and were not amplified by real-time PCR. Melt curve analysis confirmed
163 that the obtained amplicon was only the one expected in each reaction. The expression
164 levels of IL-6 relative to GAPDH were calculated using the ΔΔCq method and were
165 normalized to the control, which was arbitrarily set to a value of "1.0".

166

167 **2.5. Non-quantitative PCR**

168 Non-quantitative PCR was performed using KOD FX Neo (TOYOBO), each primer,
169 and the cDNA reaction solution obtained by the above method. The primer sequences and
170 product sizes are provided in Table S2. Thermal cycles were performed using a PC320
171 system (ASTEC, Fukuoka, Japan). Cycling conditions were 94 °C for 1 min (for initial
172 denaturation), followed by 40 cycles of denaturation (98 °C, 10 s), annealing (temperature:
173 Table S2, 10 s), and extension (68 °C, 30 s). RNAs without reverse transcription were used
174 as a negative control to examine DNA contamination. PCR products and a 100 bp DNA
175 ladder (Takara Bio) were separated on a 3% agarose gel and visualized with ethidium
176 bromide under UV illumination (Mupid-Scope WD, Mupid, Tokyo, Japan).

177

178 **2.6. Western blotting**

179 Astrocytes were lysed in RIPA buffer containing a protease inhibitor cocktail
180 (Nacalai Tesque). The samples were separated by 10% SDS-PAGE and transferred to
181 polyvinylidene difluoride membranes (Millipore, CA, USA). The membranes were blocked
182 with 5% skimmed milk and then incubated with primary antibodies at 4 °C for at least 12
183 h. Thereafter, the membranes were incubated for 1 h at room temperature (RT) with a
184 horseradish peroxidase-conjugated secondary antibody (#NA931 or #NA934, 1:3000, GE

185 Healthcare, Little Chalfont, UK). Antibody binding was visualized by ECL Prime (GE
186 Healthcare). Band intensities were measured using Fiji-ImageJ software (National
187 Institutes of Health) and normalized to the control, which was arbitrarily set to a value of
188 “1.0”.
189
190 **2.7. Enzyme-linked immunosorbent assay (ELISA)**
191 We measured the IL-6 protein levels using IL-6 ELISA Kit (#437107, Biolegend,
192 San Diego, CA, USA). The medium of cultured astrocyte treated with each drug for 6 h
193 was collected. Thereafter, the medium was centrifuged at 1,000 × g for 10 min to remove
194 dead cells and debris, and the supernatant was used for ELISA. The experiment was
195 performed according to the manufacturer's instructions and the ELISA plates were read
196 with an SH-1000 lab fluorescent microplate reader (Corona Electric Co., Ibaraki, Japan)
197 and analyzed using SF6 software (Corona Electric Co.). Quantification of astrocyte total
198 protein was performed for cells in each cultured well using the DC™ Protein Assay reagent
199 (Bio-Rad, Hercules, CA, USA). The IL-6 level was normalized by calculating the IL-6
200 protein content per astrocyte total protein content (pg/mg).
201
202 **2.8. Phalloidin staining and evaluation of astrocytic morphology *in vitro***
203 Phalloidin staining and evaluation of astrocytic morphology were conducted as

204 previously described (Kitano et al., 2021). Astrocytes cultured on coverslips were fixed
205 with 4% paraformaldehyde for 20 min at RT and then permeabilized with phosphate-
206 buffered saline containing 0.1% Triton X-100 at RT for 5 min. To stain filamentous actin
207 (F-actin), cells were incubated with Phalloidin-iFluor 488 reagent (#ab176753, 1:1000,
208 Abcam, Cambridge, UK) in phosphate-buffered saline containing 1% bovine serum
209 albumin at RT for 1 h. Coverslips were mounted onto glass slides with DAPI-Fluoromount
210 G (SouthernBiotech, Birmingham, AL, USA). Fluorescence images were obtained with a
211 fluorescence microscope (BZ-9000, KEYENCE, Osaka, Japan) using a 20× lens objective.
212 Astrocytes with process formation were defined as cells that had one or more processes
213 longer than the width of their cell bodies. The number of astrocytes with process formation
214 was visually counted using Fiji-ImageJ software. The mean percentage from more than
215 200 cells from three random images was used as one independent measurement.
216
217 **2.9. Preparation of acute hippocampal slices**
218 Male pups (14-16 days old) were anesthetized with isoflurane (Pfizer) inhalation
219 and rapidly decapitated. The brains were then quickly detached and transferred into ice-
220 cold artificial cerebrospinal fluid (ACSF) and constantly oxygenated with 95% O_2 and 5%
221 CO_2. The composition of ACSF was as follows (mM): 125 NaCl, 2.5 KCl, 2.0 $CaCl_2$, 1.0
222 $MgCl_2$, 26 $NaHCO_3$, 1.25 NaH_2PO_4, and 25 glucose (pH 7.3-7.4). The brain was glued to a

223 slicer stage (LinearSlicer Pro7, Dosaka EM, Kyoto, Japan), flooded in oxygenated cold
224 ACSF, and cut into 300 μm-thick coronal slices. The slices were incubated for 30 min at
225 22-24 °C in continuously oxygenated ACSF. Afterward, the slices, in continuously
226 oxygenated ACSF containing L(+)-ascorbic acid (200 μM), were incubated for 30 min and
227 treated with isoproterenol, dopamine, or SKF81297 for 90 min at 34 °C.
228
229 **2.10. Immunohistochemistry**
230 The slices obtained by the above method were fixed with 4% paraformaldehyde
231 for 12 h at 4 °C and then blocked for 6 h with a blocking buffer composed of 10% goat
232 serum, 0.5% Triton X-100, and 0.05% sodium azide in phosphate-buffered saline. The
233 slices were then incubated with an anti-GFAP primary antibody at 4 °C for at least 12 h
234 and incubated with an Alexa Fluor 555-conjugated goat anti-mouse antibody (#A21422,
235 1:500, Thermo Fisher Scientific, MA, USA) for 2 h at RT. The slices were mounted onto
236 glass slides with DAPI-Fluoromount G, and images were observed with a laser scanning
237 confocal microscope (LSM 700, Carl Zeiss, Oberkochen, Germany) using a 40× lens
238 objective. The CA1 areas of the hippocampus (shown in Fig. S2) were used to measure the
239 fluorescence intensity. The images (shown in Fig. 6) were used for the fluorescence
240 intensity measurements and were composed of 15 μm Z-stacks consisting of 16 optical
241 slices of 1 μm thickness by maximum intensity projection. The mean grey intensity in the

area excluding the neuronal layer was measured using Fiji-ImageJ. The results were expressed as arbitrary units.

2.11. Morphological analysis of astrocytes in hippocampal slices

Morphological features of astrocytes in the CA1 area of the hippocampus were assessed using the confocal Z-stack images obtained by immunohistochemistry. For analysis, we applied Simple Neurite Tracer, a free software plugin distributed by Fiji-ImageJ and available at (https://imagej.net/plugins/snt/), as previously described (Tavares et al., 2017). The morphological parameters assessed by Simple Neurite Tracer were the total branch length, number of branches, and average branch length. Additionally, we performed Sholl analysis, which measures the number of intersections at concentric spheres (at 4 μm intervals) originating from the soma. The mean value of 10 cells in one immunohistochemistry image was used as one independent measurement.

2.12. Data and statistical analysis

All the studies were designed to generate groups of equal size, using randomization and blinded analysis. Data are expressed as means ± S.E.M (n = number of independent measurements) of at least five independent experiments (biological replicates). After confirming that the data were normally distributed, the following tests

were performed. Statistical comparisons between the two groups were made using the unpaired Student's t-test. For all multiple comparisons, the Dunnett's test or Tukey's test was used. The Dunnett's test or Tukey's test was performed only if F achieved $p < 0.05$ and there was no significant inhomogeneity of variance by one-way ANOVA. A value of $p < 0.05$ was considered statistically significant. All statistical analysis was performed using the statistical analysis software JMP® 14 (SAS Institute, Inc., Cary, NC, USA).

3. Results

3.1. Dopamine increases IL-6 mRNA levels in astrocytes and changes astrocyte cell morphology

We first examined the effects of monoamines (dopamine, serotonin, histamine) on the mRNA levels of cytokines (IL-6, IL-1ß, tumor necrosis factor-α) and growth factors (fibroblast growth factor 2, BDNF, nerve growth factor). Serotonin and histamine (10 μM) did not affect the mRNA levels of any of the factors (Fig. 1A-F) and dopamine (10 μM) did not affect the mRNA levels of any of the factors except IL-6 (Fig. 1A-E). Conversely, treatment with dopamine for 1 h (but not 3 h) increased IL-6 mRNA levels in cerebral cortical astrocytes (Fig. 1F). In addition, dopamine for 1 h also increased IL-6 mRNA levels in hippocampal and spinal cord astrocytes (Fig. 1G).

Next, we investigated the effects of monoamines on astrocytic process formation. We previously demonstrated that noradrenaline induces processes in cultured astrocytes, which peaked after 3 h of treatment (Kitano et al., 2021). According to these results, astrocytic process formation *in vitro* was evaluated after 3 h of treatment in this study. Dopamine (10 μM for 3 h) induced process formation in hippocampal astrocytes, whereas serotonin and histamine had no effect on cell morphology (Fig. 2A and B). Furthermore, dopamine induced process formation in cerebral cortical and spinal cord astrocytes (Fig.

2C and D). Next, we confirmed the mRNA expression of dopamine receptor subtypes (D1-D5) and β-adrenoceptor subtypes (β_1-β_3) in astrocytes. Bands of all receptor subtypes were detected in cerebral cortical, hippocampal, and spinal cord astrocytes (Fig. 2E). Several molecularly distinct types of astrocytes with a region-specific distribution have been reported (Zeisel et al., 2018). However, the effects of dopamine on IL-6 mRNA levels and process formation were almost the same across different brain regions. Furthermore, there were no differences in gene expression of each receptor depending on the site of derivation. Although the cerebral cortical astrocytes are mainly used to examine the function or production mechanism of IL-6, GFAP-staining in the cerebral cortex of slice experiments was very weak (Fig. S3). Therefore, in the following experiments, cerebral cortical astrocytes were used to evaluate IL-6 expression and protein phosphorylation, and hippocampal astrocytes were used to evaluate astrocytic morphology.

3.2. Dopamine at low and high concentrations increases IL-6 mRNA levels and release via D1-like receptors and β-adrenoceptors, respectively

We investigated which receptors are involved in the dopamine-induced increase in IL-6 mRNA levels. High dopamine concentrations also act on β-adrenoceptors (Koppel et al., 2018). Therefore, we investigated the concentration-response relationships between dopamine and IL-6 mRNA levels in the presence of the β-adrenoceptor antagonist

306 propranolol. Treatment of cerebral cortical astrocytes with dopamine (1 nM to 100 μM)
307 increased IL-6 mRNA levels in a concentration-dependent manner (Fig. 3A). Propranolol
308 (10 μM) inhibited the increase in IL-6 mRNA levels induced by a high concentration of
309 dopamine (100 μM) but not that induced by a low concentration of dopamine (1 μM).
310 Dopamine (1 μM) significantly increased the IL-6 mRNA levels (Fig. 3B). In the following
311 experiments, 1 μM dopamine was used as the lowest concentration that significantly
312 increased IL-6 mRNA levels, while 100 μM dopamine was used as the high concentration
313 of dopamine that was significantly inhibited by propranolol. The D1-like receptor
314 antagonist SCH23390 (10 μM) but not the D2-like receptor antagonist haloperidol (10 μM)
315 inhibited the increase in IL-6 mRNA levels at 1 μM dopamine (Fig. 3B). The increase in
316 IL-6 mRNA levels at 100 μM dopamine was not inhibited by SCH23390, was enhanced by
317 haloperidol (Fig. 3C), and was partially inhibited by the β_1-adrenoceptor antagonist
318 atenolol (10 μM), the β_2-adrenoceptor antagonist ICI118551 (1 μM), and the β_3-
319 adrenoceptor antagonist SR59230A (1 μM) (Fig. 3D). In the presence of a mixture of
320 atenolol, ICI1118551, and SR59230A, dopamine (100 μM) failed to increase IL-6 mRNA
321 levels. Activation of D1-like receptors stimulates adenylate cyclase and phospholipase C
322 (Lee et al., 2004). IL-6 mRNA levels were increased by the D1-like receptor full agonist
323 SKF81297 (10 μM) and the D1-like receptor adenylyl cyclase agonist SKF83822 (10 μM),
324 but not by the D1-like receptor phospholipase C agonist SKF83959 (10 μM) or the D2-like

325 receptor agonist bromocriptine (10 μM) (Fig. 3E). The β-agonist isoproterenol (1 μM) and
326 the adenylate cyclase activator forskolin (10 μM) increased IL-6 mRNA levels (Fig. 3F).
327 None of the antagonists alone exerted any effect on IL-6 mRNA levels (Fig. S4A and B).
328 Next, the protein levels of IL-6 released into the culture medium were measured by ELISA.
329 Similar to the effects of dopamine on the IL-6 mRNA levels, the low (1 μM) and high (100
330 μM) concentrations of dopamine increased the release of IL-6, which were inhibited by
331 SCH23390 and propranolol, respectively (Fig. 3G and H). In addition, the release of IL-6
332 by dopamine (100 μM) was enhanced by haloperidol.
333
334 **3.3. Dopamine promotes CREB phosphorylation**
335 We have previously reported that noradrenaline increases IL-6 mRNA levels via
336 the CREB and ERK phosphorylation (Morimoto et al., 2021). Here, we investigated
337 whether low and high dopamine concentrations regulate the phosphorylation of proteins
338 involved in transcription in cerebral cortical astrocytes. Since the increase in IL-6 mRNA
339 was detected at 1 hour, we assumed that the phosphorylation of these factors occurred
340 before that, and thus we measured the phosphorylation at 30 minutes. Dopamine (1 μM
341 for 30 min) promoted CREB phosphorylation, which was inhibited by SCH23390 but not
342 by haloperidol or propranolol (Fig. 4A). Dopamine (100 μM for 30 min) also promoted
343 CREB phosphorylation, which was inhibited by SCH23390, haloperidol, and propranolol

(Fig. 4B). SKF81297, isoproterenol, and forskolin promoted CREB phosphorylation (Fig. 4C). Dopamine exerted no effect on STAT3 or mitogen-activated protein kinases (MAPKs); namely ERK, JNK, and p38 phosphorylation at low or high concentrations (Fig. 4D-G).

3.4. High dopamine concentrations regulate process formation via D2-like receptors and β- and α_2-adrenoceptors

Next, we investigated which receptors are involved in dopamine-induced process formation in hippocampal astrocytes. We used hippocampal astrocytes, but not cerebral cortical astrocytes, to investigate the evaluation of morphological changes, because GFAP-fluorescence was hardly detectable in the cerebral cortical slice. The expression level of GFAP in the cerebral cortical astrocytes is much lower than that in the hippocampus astrocytes (Zhang et al., 2019). As shown in Figure 2, there were no regional differences in the effect of dopamine and the receptor expression between the cerebral cortical and hippocampal astrocytes. Dopamine at 1 μM had no effect on process formation (Fig. 5A and B), whereas dopamine at 100 μM induced process formation (Fig. 5C and D). This effect was inhibited by propranolol but not by SCH23390. Haloperidol and the α_2-adrenoceptor antagonist atipamezole (10 μM) enhanced dopamine-induced process formation. The effect of dopamine (100 μM) was partially inhibited by atenolol, ICI118551, and SR59230A (Fig. 5E and F). SKF81297, SKF83822, isoproterenol, and forskolin, but

not SKF83959 and bromocriptine, induced process formation (Fig. 5G-J). None of the antagonists alone exerted any effect on process formation (Fig. S5).

3.5. D1-like receptor and ß-adrenoceptor agonists increase GFAP expression and change astrocytic morphology in acute hippocampal slices

We investigated whether activating dopamine receptors affects astrocytic morphology in acute hippocampal slices in addition to cultured astrocytes. Dopamine, SKF81297, and isoproterenol (10 μM for 90 min) increased the mean intensity of GFAP expression (Fig. 6A and B). Astrocytes treated with these drugs displayed increases in the total branch length and the number of branches, but not the average branch length (Fig. 6C-E). In addition, the Sholl analysis showed increases in intersections and shifts in the curve to the right, which indicates an enhanced complexity of astrocytic processes (Fig. 6F).

4. Discussion

In this study, we found that dopamine regulates IL-6 expression and process formation in astrocytes. High dopamine concentrations regulated these effects via α- and ß-adrenoceptors in addition to dopamine receptors. Furthermore, we observed bidirectional regulation, i.e., the effects of D1-like receptors and ß-adrenoceptors were negatively regulated by D2-like receptors and α_2-adrenoceptors.

Our previous study demonstrated that the noradrenaline-induced increase in IL-6 mRNA levels reached a peak 1 h after treatment (Morimoto et al., 2021). The effect of dopamine in this study was similar. After 1 h, dopamine transiently increased IL-6 mRNA levels in a concentration-dependent manner. Dopamine-induced increases in IL-6 mRNA levels were accompanied by CREB phosphorylation, which was abolished by the D1-like receptor antagonist (when 1 μM dopamine was used) and the ß-antagonist (when 100 μM dopamine was used). Furthermore, the D1-like receptor adenylyl cyclase agonist SKF83822, but not the D1-like receptor phospholipase C agonist SKF83959, increased IL-6 mRNA levels. The ß-agonist and the adenylyl cyclase activator also increased IL-6 mRNA levels. These results suggest that low dopamine concentrations act via the D1-like receptor/cAMP/CREB pathway, whereas high dopamine concentrations act via the ß-adrenoceptor/cAMP/CREB pathway to activate IL-6 transcription. These results agree with our previous study showing that the activation of ß-adrenoceptors promotes IL-6

396 transcription via the CREB pathway (Morimoto et al., 2021).

397 ERK and STAT3 phosphorylation promote IL-6 transcription in cerebral cortical
398 astrocytes (Du et al., 2020; Sun et al., 2017). However, dopamine did not affect MAPKs or
399 STAT3 phosphorylation. Therefore, these factors are unlikely to be involved in dopamine-
400 induced increases in IL-6 mRNA levels. Although the D1-like receptor antagonist partially
401 decreased dopamine (100 μM)-induced CREB phosphorylation, it had no effect on IL-6
402 mRNA levels. These effects are likely due to the potent effect of dopamine via ß-
403 adrenoceptors, and CREB phosphorylation above a certain level may not contribute to the
404 increase in IL-6 mRNA levels. Furthermore, the D2-like receptor antagonists further
405 enhanced dopamine (100 μM)-induced IL-6 mRNA increases, suggesting that D2-like
406 receptors exert a suppressive effect on IL-6 transcription in the presence of high dopamine
407 concentrations. Contrary to this result, D2-like receptor antagonists suppressed dopamine
408 (100 μM)-induced CREB phosphorylation. Therefore, other pathways are likely to be
409 involved in this suppressive effect.

410 Dopamine (100 μM) induced astrocytic process formation, which was abolished by
411 a ß-antagonist. Conversely, an α_2-antagonist enhanced dopamine-induced process
412 formation. As we previously reported, the activation of ß-adrenoceptors induces astrocytic
413 process formation via cAMP signaling, whereas the activation of α_2-adrenoceptors inhibits
414 both cAMP-dependent and -independent astrocytic process formation (Kitano et al., 2021).

In this study, we showed that the effects of dopamine on process formation were also regulated by β- and α_2-adrenoceptors. In addition, the D1-like receptor agonist induced process formation, and the D2-like receptor antagonist enhanced dopamine-induced process formation. Therefore, D1- and D2-like receptors are likely to play a role in the bidirectional regulation of process formation by dopamine.

It has been reported that the dephosphorylation of myosin light chains by down-regulation of the Rho pathway is involved in the mechanism of intracellular cAMP-induced process formation (Rodnight and Gottfried, 2013). Therefore, the dopamine-induced increase in IL-6 mRNA and process formation is likely to occur by different intracellular pathways, and these could be a reason to explain the difference between the duration of dopamine effect on IL-6 mRNA (1 h, but not 3 h) and that on process formation (3 h).

The effect of β-adrenoceptor agonists on astrocytic processes have been observed in brain slices *in situ* (Sherpa et al., 2016), *in vivo* (Hodges-Savola et al., 1996; Sutin and Griffith, 1993), and in cultured astrocytes *in vitro* (Kitano et al., 2021). The adenylate cyclase activator forskolin increases the overall thickness of the primary processes in the hippocampal slice (Ujita et al., 2017). In this study, we found that dopamine or the D1-like receptor agonist changed astrocytic morphology and upregulated GFAP expression in acute hippocampal slices, suggesting that dopamine receptors are involved in modulating

434 astrocytic morphology *in vivo*. IL-6 upregulation may contribute to dopamine-induced
435 morphological changes in astrocytes. However, it has been reported that the morphology
436 of astrocytes in GFAP-IL6 transgenic mice does not differ from that in normal mice, even
437 though GFAP-IL6 transgenic mice exhibit high IL-6 expression in astrocytes (Penkowa et
438 al., 2003). Therefore, IL-6 is not likely to exert effects on astrocytic morphology.

439 Dopamine is a direct precursor in the synthesis of noradrenaline, and thus
440 dopamine and noradrenaline are structurally similar. Whereas dopamine and
441 noradrenaline normally only interact with their respective receptors, they can also
442 interact with each other's receptors (Lei, 2014). Dopamine has been shown to activate all
443 adrenoceptor subtypes expressed in Chinese hamster ovary cells (Zhang et al., 2004).
444 Intravenously administered dopamine at low doses activates dopamine receptors in blood
445 vessels, whereas dopamine at higher doses activates mainly adrenoceptors (Frishman and
446 Hotchkiss, 1996). These findings support our results, namely, that dopamine at low
447 concentrations acted on dopamine receptors, whereas dopamine at high concentrations
448 acted mainly on adrenoceptors in astrocytes.

449 Adrenergic and dopamine receptors can form homodimers and heterodimers
450 (Franco et al., 2000). The dimerization may lead to different properties from the monomers.
451 For example, D2-like and β_2 adrenergic receptors form homodimers, which transduce
452 enhanced signals compared to monomers (Hebert et al., 1996; Wouters et al., 2019).

453 Furthermore, D2-like receptors form heterodimers with β_2 adrenergic receptors and
454 enhance adenylate cyclase activity when stimulated by dopamine (Rebois et al., 2012;
455 Watts and Neve, 1997). A dopamine D2 receptor antagonist decreases the level of D2-like
456 receptors dimer formation (Wouters et al., 2019). In addition, an adenosine A1 receptor
457 antagonist enhances the activation of the dopamine D1 receptor coupled with the A1
458 receptor (Franco et al., 2000). Therefore, the antagonists used in this study may affect not
459 only monometric receptors but also receptor complexes. Further studies are needed to
460 address this issue.

461 In this study, the D2-like, but not the D1-like, receptor antagonist had no effects
462 on the dopamine (1 μM)-induced increase in IL-6 mRNA levels. D2-like receptors have a
463 higher affinity for dopamine (Seeman and Grigoriadis, 1987); however, D2-like receptor
464 expression is lower than D1-like receptor expression in at least 21 brain regions (Richfield
465 et al., 1989). In a simulation with model parameters for dopamine receptors in striatal
466 neurons, the amount of dopamine binding to D2-like receptors was approximately 10 times
467 lower than that to D1-like receptors in the presence of 1 μM dopamine (Hunger et al.,
468 2020). The D2-like receptor antagonist may not have exerted any effect because of the low
469 numbers of D2-like receptors available for dopamine binding.

470 The concentration of dopamine in human cerebrospinal fluid *in vivo* has been
471 reported to be 39.5 ± 19.8 nM (Strittmatter et al., 1997), while the concentration of

dopamine in the synaptic gap reaches 10-100 μM (Cragg and Rice, 2004; Koppel et al., 2018), and astrocytic processes contact neurons and synaptic gaps (i.e., the "tripartite synapse"), thus regulating synaptic function (Allen and Eroglu, 2017). Furthermore, dopamine concentrations increase under acute stress and ischemic conditions (Baker et al., 1991; Chang et al., 1993; Pascucci et al., 2007). Rat models of drug abuse and pathological gamblers have higher dopamine levels than healthy groups (Egenrieder et al., 2020; van Holst et al., 2018). It is likely that dopamine concentrations (1-100 μM) used in this study could be reached, at least transiently, *in vivo* under physiological and pathological conditions. Further investigations are needed to evaluate the effects of brief exposure of astrocytes to dopamine.

In this study, dopamine (1 μM) increased IL-6 mRNA levels and release via D1-like receptors. IL-6 has been widely reported to play a beneficial role in brain function, e.g., by acting as a neurotrophic factor (Wagner, 1996), suppressing neuronal cell death (Day et al., 2014), and improving learning and memory impairment after traumatic brain injury (Willis et al., 2020). Furthermore, the D1-like agonist SKF83959 is suggested to protect nigral neurons from MPTP neurotoxicity via astrocytic D1-like receptors (Zhang et al., 2009). In addition, the activation of astrocytic D1-like receptors enhances the recovery of brain function after experimental stroke (Kuric et al., 2013). As IL-6 and D1-like receptors appear to contribute to recovery from various diseases, the effects of low

dopamine concentrations on IL-6 transcription via astrocytic D1-like receptors may be beneficial. Conversely, high dopamine concentrations are likely to cause CNS inflammation and induce reactive astrocytes. In this study, dopamine (100 μM) induced morphological changes in astrocytic cultures and acute brain slices, and increased GFAP expression in astrocytes in acute brain slices. These characteristics are consistent with those of reactive astrocytes in CNS inflammation, including elongated and complex processes and increased GFAP expression (Pekny and Pekna, 2014). Dopamine and IL-6 levels increase under ischemic conditions (Baker et al., 1991; Chang et al., 1993; Clark et al., 1999). In addition, astrocytes upregulate ß-adrenoceptors and downregulate α_2-adrenoceptors in neurodegenerative diseases (Mantyh et al., 1995; Shao and Sutin, 1992). Taken together, adrenoceptors in astrocytes may be involved in the pathogenesis of neuroinflammatory diseases associated with extremely elevated dopamine levels. Thus, the inhibitory role of dopamine via D2-like receptors and α_2-adrenoceptors may improve such pathological conditions.

CRediT authorship contribution statement

Kohei Morimoto: Conceptualization, Formal analysis, Investigation, Writing - original draft, Visualization, Funding acquisition. **Mai Ouchi**: Formal analysis, Investigation, Writing - original draft. **Taisuke Kitano**: Conceptualization, Writing - review & editing. **Ryota Eguchi**: Conceptualization, Writing - review & editing, Funding acquisition. **Ken-ichi Otsuguro**: Conceptualization, Writing - review & editing, Supervision, Funding acquisition.

Declaration of Competing Interest

The authors declare that they have no known competing financial interests or personal relationships that could have appeared to influence the work reported in this paper.

Acknowledgments

This work was supported by JSPS KAKENHI Grant Numbers 19K23701 and 21K05950 and the World-leading Innovative and Smart Education (WISE) Program (1801) from the Ministry of Education, Culture, Sports, Science, and Technology, Japan.

References

Allen, N.J., Eroglu, C., 2017. Cell Biology of Astrocyte-Synapse Interactions. Neuron 96, 697–708. https://doi.org/10.1016/J.NEURON.2017.09.056

Baker, A.J., Zornow, M.H., Scheller, M.S., Yaksh, T.L., Skilling, S.R., Smullin, D.H., Larson, A.A., Kuczenski, R., 1991. Changes in Extracellular Concentrations of Glutamate, Aspartate, Glycine, Dopamine, Serotonin, and Dopamine Metabolites After Transient Global Ischemia in the Rabbit Brain. Journal of Neurochemistry 57, 1370–1379. https://doi.org/10.1111/j.1471-4159.1991.tb08303.x

Chang, C.J., Ishii, H., Yamamoto, H., Yamamoto, T., Spatz, M., 1993. Effects of Cerebral Ischemia on Regional Dopamine Release and D1 and D2 Receptors. Journal of Neurochemistry 60, 1483–1490. https://doi.org/10.1111/j.1471-4159.1993.tb03311.x

Clark, W.M., Rinker, L.G., Lessov, N.S., Hazel, K., Eckenstein, F., 1999. Time course of IL-6 expression in experimental CNS ischemia. Neurological Research 21. https://doi.org/10.1080/01616412.1999.11740933

Corkrum, M., Covelo, A., Lines, J., Bellocchio, L., Pisansky, M., Loke, K., Quintana, R., Rothwell, P.E., Lujan, R., Marsicano, G., Martin, E.D., Thomas, M.J., Kofuji, P., Araque, A., 2020. Dopamine-Evoked Synaptic Regulation in the Nucleus Accumbens Requires Astrocyte Activity. Neuron 105, 1036-1047.e5. https://doi.org/10.1016/j.neuron.2019.12.026

543 Cragg, S.J., Rice, M.E., 2004. DAncing past the DAT at a DA synapse. Trends in
544 Neurosciences 27, 270–277. https://doi.org/10.1016/J.TINS.2004.03.011
545 Day, J.S., O'Neill, E., Cawley, C., Aretz, N.K., Kilroy, D., Gibney, S.M., Harkin, A., Connor,
546 T.J., 2014. Noradrenaline acting on astrocytic ß2-adrenoceptors induces neurite
547 outgrowth in primary cortical neurons. Neuropharmacology 77, 234–248.
548 https://doi.org/10.1016/j.neuropharm.2013.09.027
549 Descarries, L., Lemay, B., Doucet, G., Berger, B., 1987. Regional and laminar density of
550 the dopamine innervation in adult rat cerebral cortex. Neuroscience 21, 807–824.
551 https://doi.org/10.1016/0306-4522(87)90038-8
552 Du, L., Chang, H., Xu, W., Wei, Y., Wang, Y., Yin, L., Zhang, X., 2020. Effect of NMO-IgG
553 on the interleukin-6 cascade in astrocytes via activation of the JAK/STAT3 signaling
554 pathway. Life Sciences 258. https://doi.org/10.1016/j.lfs.2020.118217
555 Edelmann, E., Lessmann, V., 2018. Dopaminergic innervation and modulation of
556 hippocampal networks. Cell and Tissue Research 373, 711–727.
557 https://doi.org/10.1007/s00441-018-2800-7
558 Egenrieder, L., Mitricheva, E., Spanagel, R., Noori, H.R., 2020. No basal or drug-induced
559 sex differences in striatal dopaminergic levels: a cluster and meta-analysis of rat
560 microdialysis studies. Journal of Neurochemistry 152, 482–492.
561 https://doi.org/10.1111/jnc.14911

562 Escartin, C., Galea, E., Lakatos, A., O'Callaghan, J.P., Petzold, G.C., Serrano-Pozo, A.,
563 Steinhäuser, C., Volterra, A., Carmignoto, G., Agarwal, A., Allen, N.J., Araque, A.,
564 Barbeito, L., Barzilai, A., Bergles, D.E., Bonvento, G., Butt, A.M., Chen, W.T., Cohen-
565 Salmon, M., Cunningham, C., Deneen, B., De Strooper, B., Díaz-Castro, B., Farina,
566 C., Freeman, M., Gallo, V., Goldman, J.E., Goldman, S.A., Götz, M., Gutiérrez, A.,
567 Haydon, P.G., Heiland, D.H., Hol, E.M., Holt, M.G., Iino, M., Kastanenka, K. V.,
568 Kettenmann, H., Khakh, B.S., Koizumi, S., Lee, C.J., Liddelow, S.A., MacVicar, B.A.,
569 Magistretti, P., Messing, A., Mishra, A., Molofsky, A. V., Murai, K.K., Norris, C.M.,
570 Okada, S., Oliet, S.H.R., Oliveira, J.F., Panatier, A., Parpura, V., Pekna, M., Pekny,
571 M., Pellerin, L., Perea, G., Pérez-Nievas, B.G., Pfrieger, F.W., Poskanzer, K.E.,
572 Quintana, F.J., Ransohoff, R.M., Riquelme-Perez, M., Robel, S., Rose, C.R., Rothstein,
573 J.D., Rouach, N., Rowitch, D.H., Semyanov, A., Sirko, S., Sontheimer, H., Swanson,
574 R.A., Vitorica, J., Wanner, I.B., Wood, L.B., Wu, J., Zheng, B., Zimmer, E.R., Zorec, R.,
575 Sofroniew, M. V., Verkhratsky, A., 2021. Reactive astrocyte nomenclature, definitions,
576 and future directions. Nature Neuroscience 24, 312–325.
577 https://doi.org/10.1038/s41593-020-00783-4

578 Franco, R., Ferre, S., Agnati, L., Torvinen, M., Gines, S., Hillion, J., Casado, V., Lledo, P.-
579 M., Zoli, M., Lluis, C., Fuxe, K., 2000. Evidence for Adenosine/Dopamine Receptor
580 Interactions: Indications for Heteromerization. Neuropsychopharmacology 23, S50–

S59. https://doi.org/10.1016/S0893-133X(00)00144-5

Frishman, W.H., Hotchkiss, H., 1996. Selective and nonselective dopamine receptor agonists: An innovative approach to cardiovascular disease treatment. American Heart Journal 132, 861–870. https://doi.org/10.1016/S0002-8703(96)90323-3

Fuxe, K., Agnati, L.F., Marcoli, M., Borroto-Escuela, D.O., 2015. Volume Transmission in Central Dopamine and Noradrenaline Neurons and Its Astroglial Targets. Neurochemical Research 40. https://doi.org/10.1007/s11064-015-1574-5

Gruol, D.L., Nelson, T.E., 1997. Physiological and pathological roles of interleukin-6 in the central nervous system. Molecular Neurobiology 15, 307–339. https://doi.org/10.1007/BF02740665

Hart, C.G., Karimi-Abdolrezaee, S., 2021. Recent insights on astrocyte mechanisms in CNS homeostasis, pathology, and repair. Journal of Neuroscience Research 99, 2427–2462. https://doi.org/https://doi.org/10.1002/jnr.24922

Hebert, T.E., Moffett, S., Morello, J.-P., Loisel, T.P., Bichet, D.G., Barret, C., Bouvier, M., 1996. A Peptide Derived from a ß2-Adrenergic Receptor Transmembrane Domain Inhibits Both Receptor Dimerization and Activation*. Journal of Biological Chemistry 271, 16384–16392. https://doi.org/https://doi.org/10.1074/jbc.271.27.16384

Hertz, L., Lovatt, D., Goldman, S.A., Nedergaard, M., 2010. Adrenoceptors in brain: Cellular gene expression and effects on astrocytic metabolism and [Ca2+]i.

Neurochemistry International 57, 411–420. https://doi.org/10.1016/j.neuint.2010.03.019

Hodges-Savola, C., Rogers, S.D., Ghilardi, J.R., Timm, D.R., Mantyh, P.W., 1996. ß-Adrenergic receptors regulate astrogliosis and cell proliferation in the central nervous system in vivo. Glia 17, 52–62. https://doi.org/10.1002/(SICI)1098-1136(199605)17:1<52::AID-GLIA5>3.0.CO;2-9

Hunger, L., Kumar, A., Schmidt, R., 2020. Abundance compensates kinetics: Similar effect of dopamine signals on D1 and D2 receptor populations. Journal of Neuroscience 40, 2868–2881. https://doi.org/10.1523/JNEUROSCI.1951-19.2019

John, G.R., Lee, S.C., Brosnan, C.F., 2003. Cytokines: Powerful regulators of glial cell activation. Neuroscientist. https://doi.org/10.1177/1073858402239587

Kitano, T., Eguchi, R., Okamatsu-Ogura, Y., Yamaguchi, S., Otsuguro, K. ichi, 2021. Opposing functions of α- and ß-adrenoceptors in the formation of processes by cultured astrocytes. Journal of Pharmacological Sciences 145, 228–240. https://doi.org/10.1016/J.JPHS.2020.12.005

Klein, M.O., Battagello, D.S., Cardoso, A.R., Hauser, D.N., Bittencourt, J.C., Correa, R.G., 2019. Dopamine: Functions, Signaling, and Association with Neurological Diseases. Cellular and Molecular Neurobiology. https://doi.org/10.1007/s10571-018-0632-3

Koppel, I., Jaanson, K., Klasche, A., Tuvikene, J., Tiirik, T., Pärn, A., Timmusk, T., 2018.

Dopamine cross-reacts with adrenoreceptors in cortical astrocytes to induce BDNF expression, CREB signaling and morphological transformation. GLIA 66, 206–216. https://doi.org/10.1002/glia.23238

Kuric, E., Wieloch, T., Ruscher, K., 2013. Dopamine receptor activation increases glial cell line-derived neurotrophic factor in experimental stroke. Experimental Neurology 247, 202–208. https://doi.org/10.1016/j.expneurol.2013.04.016

Lee, S.P., So, C.H., Rashid, A.J., Varghese, G., Cheng, R., Lança, A.J., O'Dowd, B.F., George, S.R., 2004. Dopamine D1 and D2 receptor co-activation generates a novel phospholipase C-mediated calcium signal. Journal of Biological Chemistry 279, 35671–35678. https://doi.org/10.1074/jbc.M401923200

Lei, S., 2014. Cross interaction of dopaminergic and adrenergic systems in neural modulation. International Journal of Physiology, Pathophysiology and Pharmacology 6, 137–142.

Mantyh, P.W., Rogers, S.D., Allen, C.J., Catton, M.D., Ghilardi, J.R., Levin, L.A., Maggio, J.E., Vigna, S.R., 1995. ß2-Adrenergic Receptors Are Expressed By Glia in Vivo in the Normal and Injured Central Nervous System in the Rat, Rabbit, and Human. Journal of Neuroscience 15, 152–164. https://doi.org/10.1523/jneurosci.15-01-00152.1995

Miyazaki, I., Asanuma, M., Diaz-Corrales, F.J., Miyoshi, K., Ogawa, N., 2004. Direct evidence for expression of dopamine receptors in astrocytes from basal ganglia. Brain

638 Research 1029, 120–123. https://doi.org/10.1016/j.brainres.2004.09.014
639 Montoya, A., Elgueta, D., Campos, J., Chovar, O., Falcón, P., Matus, S., Alfaro, I., Bono,
640 M.R., Pacheco, R., 2019. Dopamine receptor D3 signalling in astrocytes promotes
641 neuroinflammation. Journal of Neuroinflammation 16, 1–19.
642 https://doi.org/10.1186/s12974-019-1652-8
643 Morimoto, K., Eguchi, R., Kitano, T., Otsuguro, K., 2021. Alpha and beta adrenoceptors
644 activate interleukin-6 transcription through different pathways in cultured
645 astrocytes from rat spinal cord. Cytokine 142, 155497.
646 https://doi.org/10.1016/j.cyto.2021.155497
647 Morimoto, K., Kitano, T., Eguchi, R., Otsuguro, K., 2020. Bidirectional modulation of TNF-
648 α transcription via α- and ß-adrenoceptors in cultured astrocytes from rat spinal cord.
649 Biochemical and Biophysical Research Communications 528, 78–84.
650 https://doi.org/10.1016/j.bbrc.2020.05.011
651 Pascucci, T., Ventura, R., Latagliata, E.C., Cabib, S., Puglisi-Allegra, S., 2007. The medial
652 prefrontal cortex determines the accumbens dopamine response to stress through the
653 opposing influences of norepinephrine and dopamine. Cerebral Cortex 17, 2796–2804.
654 https://doi.org/10.1093/cercor/bhm008
655 Pekny, M., Nilsson, M., 2005. Astrocyte activation and reactive gliosis. Glia 50, 427–434.
656 https://doi.org/10.1002/glia.20207

657 Pekny, M., Pekna, M., 2014. Astrocyte reactivity and reactive astrogliosis: Costs and
658 benefits. Physiological Reviews 94, 1077–1098.
659 https://doi.org/10.1152/physrev.00041.2013
660 Penkowa, M., Giralt, M., Lago, N., Camats, J., Carrasco, J., Hernández, J., Molinero, A.,
661 Campbell, I.L., Hidalgo, J., 2003. Astrocyte-targeted expression of IL-6 protects the
662 CNS against a focal brain injury. Experimental Neurology 181, 130–148.
663 https://doi.org/10.1016/S0014-4886(02)00051-1
664 Percie du Sert, N., Hurst, V., Ahluwalia, A., Alam, S., Avey, M.T., Baker, M., Browne, W.J.,
665 Clark, A., Cuthill, I.C., Dirnagl, U., Emerson, M., Garner, P., Holgate, S.T., Howells,
666 D.W., Karp, N.A., Lazic, S.E., Lidster, K., MacCallum, C.J., Macleod, M., Pearl, E.J.,
667 Petersen, O.H., Rawle, F., Reynolds, P., Rooney, K., Sena, E.S., Silberberg, S.D.,
668 Steckler, T., Wuerbel, H., 2020. The ARRIVE guidelines 2.0: updated guidelines for
669 reporting animal research. BMJ Open Science 4, e100115.
670 https://doi.org/10.1136/bmjos-2020-100115
671 Rebois, R.V., Maki, K., Meeks, J.A., Fishman, P.H., Hébert, T.E., Northup, J.K., 2012. D2-
672 like dopamine and ß-adrenergic receptors form a signaling complex that integrates
673 Gs- and Gi-mediated regulation of adenylyl cyclase. Cellular Signalling 24, 2051–
674 2060. https://doi.org/https://doi.org/10.1016/j.cellsig.2012.06.011
675 Richfield, E.K., Penney, J.B., Young, A.B., 1989. Anatomical and affinity state comparisons

676 between dopamine D1 and D2 receptors in the rat central nervous system.
677 Neuroscience 30, 767–777. https://doi.org/10.1016/0306-4522(89)90168-1
678 Ridet, J.L., Sandillon, F., Rajaofetra, N., Geffard, M., Privat, A., 1992. Spinal dopaminergic
679 system of the rat: light and electron microscopic study using an antiserum against
680 dopamine, with particular emphasis on synaptic incidence. Brain Research 598, 233–
681 241. https://doi.org/10.1016/0006-8993(92)90188-F
682 Rodnight, R.B., Gottfried, C., 2013. Morphological plasticity of rodent astroglia. Journal
683 of Neurochemistry 124, 263–275. https://doi.org/10.1111/jnc.12087
684 Schiweck, J., Murk, K., Ledderose, J., Münster-Wandowski, A., Ornaghi, M., Vida, I.,
685 Eickholt, B.J., 2021. Drebrin controls scar formation and astrocyte reactivity upon
686 traumatic brain injury by regulating membrane trafficking. Nature Communications
687 12. https://doi.org/10.1038/s41467-021-21662-x
688 Seeman, P., Grigoriadis, D., 1987. Dopamine receptors in brain and periphery.
689 Neurochemistry International 10, 1–25. https://doi.org/10.1016/0197-0186(87)90167-
690 7
691 Shao, Y., Sutin, J., 1992. Expression of adrenergic receptors in individual astrocytes and
692 motor neurons isolated from the adult rat brain. Glia 6.
693 https://doi.org/10.1002/glia.440060205
694 Sherpa, A.D., Xiao, F., Joseph, N., Aoki, C., Hrabetova, S., 2016. Activation of ß-adrenergic

695 receptors in rat visual cortex expands astrocytic processes and reduces extracellular
696 space volume. Synapse 70, 307–316. https://doi.org/10.1002/syn.21908
697 Sofroniew, M. V., 2009. Molecular dissection of reactive astrogliosis and glial scar
698 formation. Trends in Neurosciences 32, 638–647.
699 https://doi.org/10.1016/j.tins.2009.08.002
700 Stogsdill, J.A., Ramirez, J., Liu, D., Kim, Y.H., Baldwin, K.T., Enustun, E., Ejikeme, T., Ji,
701 R.R., Eroglu, C., 2017. Astrocytic neuroligins control astrocyte morphogenesis and
702 synaptogenesis. Nature 551, 192–197. https://doi.org/10.1038/nature24638
703 Strittmatter, M., Grauer, M., Isenberg, E., Hamann, G., Fischer, C., Hoffmann, K.H., Blaes,
704 F., Schimrigk, K., 1997. Cerebrospinal fluid neuropeptides and monoaminergic
705 transmitters in patients with trigeminal neuralgia. Headache 37, 211–216.
706 https://doi.org/10.1046/j.1526-4610.1997.3704211.x
707 Sun, L., Li, Yan, Jia, X., Wang, Q., Li, Yue, Hu, M., Tian, L., Yang, J., Xing, W., Zhang, W.,
708 Wang, J., Xu, H., Wang, L., Zhang, D., Ren, H., 2017. Neuroprotection by IFN-γ via
709 astrocyte-secreted IL-6 in acute neuroinflammation. Oncotarget 8, 40065–40078.
710 https://doi.org/10.18632/oncotarget.16990
711 Sutin, J., Griffith, R., 1993. B-Adrenergic Receptor Blockade Suppresses Glial Scar
712 Formation. Experimental Neurology. https://doi.org/10.1006/exnr.1993.1056
713 Tavares, G., Martins, M., Correia, J.S., Sardinha, V.M., Guerra-Gomes, S., das Neves, S.P.,

714 Marques, F., Sousa, N., Oliveira, J.F., 2017. Employing an open-source tool to assess
715 astrocyte tridimensional structure. Brain Structure and Function 222, 1989–1999.
716 https://doi.org/10.1007/s00429-016-1316-8
717 Ujita, S., Sasaki, T., Asada, A., Funayama, K., Gao, M., Mikoshiba, K., Matsuki, N.,
718 Ikegaya, Y., 2017. cAMP-Dependent Calcium Oscillations of Astrocytes: An
719 Implication for Pathology. Cereb Cortex 27, 1602–1614.
720 https://doi.org/10.1093/cercor/bhv310
721 van Holst, R.J., Sescousse, G., Janssen, L.K., Janssen, M., Berry, A.S., Jagust, W.J., Cools,
722 R., 2018. Increased Striatal Dopamine Synthesis Capacity in Gambling Addiction.
723 Biological Psychiatry 83, 1036–1043. https://doi.org/10.1016/j.biopsych.2017.06.010
724 Wagner, J.A., 1996. Is IL-6 both a cytokine and a neurotrophic factor? Journal of
725 Experimental Medicine. https://doi.org/10.1084/jem.183.6.2417
726 Watts, V.J., Neve, K.A., 1997. Activation of Type II Adenylate Cyclase by D2 and D4 but
727 Not D3 Dopamine Receptors. Molecular Pharmacology 52, 181.
728 https://doi.org/10.1124/mol.52.2.181
729 Willis, E.F., MacDonald, K.P.A., Nguyen, Q.H., Garrido, A.L., Gillespie, E.R., Harley,
730 S.B.R., Bartlett, P.F., Schroder, W.A., Yates, A.G., Anthony, D.C., Rose-John, S.,
731 Ruitenberg, M.J., Vukovic, J., 2020. Repopulating Microglia Promote Brain Repair in
732 an IL-6-Dependent Manner. Cell 180, 833-846.e16.

https://doi.org/10.1016/j.cell.2020.02.013

Wouters, E., Marín, A.R., Dalton, J.A.R., Giraldo, J., Stove, C., 2019. Distinct dopamine D2 receptor antagonists differentially impact D2 receptor oligomerization. International Journal of Molecular Sciences 20. https://doi.org/10.3390/ijms20071686

Zeisel, A., Hochgerner, H., Lönnerberg, P., Johnsson, A., Memic, F., van der Zwan, J., Häring, M., Braun, E., Borm, L.E., la Manno, G., Codeluppi, S., Furlan, A., Lee, K., Skene, N., Harris, K.D., Hjerling-Leffler, J., Arenas, E., Ernfors, P., Marklund, U., Linnarsson, S., 2018. Molecular Architecture of the Mouse Nervous System. Cell 174, 999-1014.e22. https://doi.org/10.1016/J.CELL.2018.06.021

Zhang, W.P., Ouyang, M., Thomas, S.A., 2004. Potency of catecholamines and other L-tyrosine derivatives at the cloned mouse adrenergic receptors. Neuropharmacology 47, 438–449. https://doi.org/10.1016/j.neuropharm.2004.04.017

Zhang, X., Zhou, Z., Wang, D., Li, A., Yin, Y., Gu, X., Ding, F., Zhen, X., Zhou, J., 2009. Activation of phosphatidylinositol-linked D1-like receptor modulates FGF-2 expression in astrocytes via IP3-dependent Ca2+ signaling. Journal of Neuroscience 29, 7766–7775. https://doi.org/10.1523/JNEUROSCI.0389-09.2009

Zhang, Z., Ma, Z., Zou, W., Guo, H., Liu, M., Ma, Y., Zhang, L., 2019. The Appropriate Marker for Astrocytes: Comparing the Distribution and Expression of Three Astrocytic Markers in Different Mouse Cerebral Regions. BioMed Research

International 2019. https://doi.org/10.1155/2019/9605265

Zhu, J., Hu, Z., Han, X., Wang, D., Jiang, Q., Ding, J., Xiao, M., Wang, C., Lu, M., Hu, G., 2018. Dopamine D2 receptor restricts astrocytic NLRP3 inflammasome activation via enhancing the interaction of ß-arrestin2 and NLRP3. Cell Death and Differentiation 25, 2037–2049. https://doi.org/10.1038/s41418-018-0127-2

759 **Figure legends**

760

761 **Figure 1. The effects of monoamines on mRNA levels of multiple factors and cell**

762 **morphology in cultured astrocytes.**

763 (A-F) The mRNA levels of tumor necrosis factor-α (A), IL-1β (B), nerve growth factor (C),

764 brain-derived neurotrophic factor (D), fibroblast growth factor 2 (E), and IL-6 (F) in

765 cerebral cortical astrocytes treated with serotonin (5-HT, 10 μM), histamine (HA, 10 μM),

766 and dopamine (DA, 10 μM) for 1 and 3 h. The mRNA levels of each factor were normalized

767 to the control level, which was arbitrarily set to a value of "1.0". $^{**}p < 0.01$ vs. control

768 (Dunnett's test), n = 6. (G) IL-6 mRNA levels in hippocampal and spinal cord astrocytes

769 treated with DA (10 μM) for 1 h. $^{**}p < 0.01$ (unpaired Student's t-test), n = 6. All data are

770 presented as means ± S.E.M.

771

772 **Figure 2. The effects of dopamine on IL-6 mRNA levels, process formation, and receptor**

773 **expression in astrocytes from different brain regions.**

774 (A, B) Representative images of F-actin (green) and DAPI (blue) in hippocampal astrocytes

775 treated with serotonin (5-HT, 10 μM), histamine (HA, 10 μM), and dopamine (DA, 10 μM)

776 for 3 h (A). Scale bars = 100 μm. The percentage of cells with process formation (B). More

777 than 200 cells in three random fields were counted. $^{**}p < 0.01$ vs. control (Dunnett's test),

778 n = 6. (C, D) Representative images of F-actin (green) and DAPI (blue) in cerebral cortical
779 and spinal cord astrocytes treated with DA (10 μM) for 3 h (C). Scale bars = 100 μm. The
780 percentage of cells with process formation (D). More than 200 cells in three random fields
781 were counted. $^{**}p < 0.01$ (unpaired Student's t-test), n = 6. All data are presented as means
782 ± S.E.M. (E) Bands for all dopamine receptor and adrenoceptor subtypes were detected in
783 cerebral cortical (upper), hippocampal (middle), and spinal cord (lower) astrocytes. RT (+)
784 and (–) indicates samples reverse-transcribed (+) or not (–), respectively.
785
786 **Figure 3. The effects of dopamine receptor and adrenoceptor agonists or antagonists on**
787 **IL-6 mRNA levels and release.**
788 (A) IL-6 mRNA levels in cerebral cortical astrocytes treated with dopamine (DA, 1 nM to
789 100 μM) in the presence or absence of the β-antagonist propranolol (PROP, 10 μM) for 1 h.
790 $^{**}p < 0.01$ (unpaired Student's t-test), n = 6. (B-D) IL-6 mRNA levels in astrocytes treated
791 with DA (B: 1 μM, C and D: 100 μM) in the presence or absence of the D1-like receptor
792 antagonist SCH23390 (SCH, 10 μM), D2-like receptor antagonist haloperidol (HAL, 10
793 μM), PROP (10 μM), β_1-adrenoceptor antagonist atenolol (ATE, 10 μM), β_2-adrenoceptor
794 antagonist ICI118551 (ICI, 1 μM), and β_3-adrenoceptor antagonist SR59230A (SR, 1 μM)
795 for 1 h. n.s.: not significant, $^{*}p < 0.05$, $^{**}p < 0.01$ (vs. DA alone, B and C, Dunnett's test),
796 (D, Tukey's t-test), n = 6. (E, F) IL-6 mRNA levels in astrocytes treated with the D1-like

receptor full agonist SKF81297 (10 μM), D1-like receptor adenylyl cyclase agonist SKF83822 (10 μM), D1-like receptor phospholipase C agonist SKF83959 (10 μM), D2-like receptor agonist bromocriptine (BRO, 10 μM), β-agonist isoproterenol (ISO, 1 μM), or adenylate cyclase activator forskolin (FSK, 10 μM) for 1 h. *$p < 0.05$, **$p < 0.01$ vs. control (Dunnett's test), n = 6. (G, H) IL-6 protein levels of the medium were measured by ELISA. Astrocyte was treated with each drug for 6 h. IL-6 levels were normalized by astrocyte total protein. *$p < 0.05$, **$p < 0.01$ vs. DA alone (Dunnett's test), n = 5. All data are presented as means ± S.E.M.

Figure 4. The effects of dopamine receptor and adrenoceptor agonists or antagonists on CREB, MAPKs, and STAT3 phosphorylation.

(A-C) The protein expression levels of phosphorylated and total CREB were quantified, and representative blots are shown. Cerebral cortical astrocytes were treated with dopamine (A: 1 μM, B: 100 μM), D1-like receptor full agonist SKF81297 (10 μM), β-agonist isoproterenol (ISO, 1 μM), and adenylate cyclase activator forskolin (FSK, 10 μM) in the presence or absence of the D1-like receptor antagonist SCH23390 (SCH, 10 μM), D2-like receptor antagonist haloperidol (HAL, 10 μM), and β-antagonist propranolol (PROP, 10 μM) for 30 min. *$p < 0.05$, **$p < 0.01$ (vs. DA alone, A and B, Dunnett's test), (vs. control, C, Dunnett's test), n = 6. (D-G) The protein expression levels of phosphorylated and total

816 ERK (D), JNK (E), p38 (F), and STAT3 (G) were quantified, and representative blots are
817 shown. Astrocytes were treated with dopamine (1 or 100 μM), n = 6. All data are presented
818 as means ± S.E.M.
819
820 **Figure 5. The effects of dopamine receptor and adrenoceptor agonists or antagonists on**
821 **astrocytic process formation.**
822 (A, C, E, G, I) Representative images of F-actin (green) and DAPI (blue) in hippocampal
823 astrocytes treated with dopamine (DA, A: 1 μM, C and E: 100 μM), D1-like receptor full
824 agonist SKF81297 (10 μM), D1-like receptor adenylyl cyclase agonist SKF83822 (10 μM),
825 D1-like receptor phospholipase C agonist SKF83959 (10 μM), D2-like receptor agonist
826 bromocriptine (BRO, 10 μM), β-agonist isoproterenol (ISO, 1 μM), and adenylate cyclase
827 activator forskolin (FSK, 10 μM) in the presence or absence of the D1-like receptor
828 antagonist SCH23390 (SCH, 10 μM), D2-like receptor antagonist haloperidol (HAL, 10
829 μM), β-adrenoceptor antagonist (PROP, 10 μM), α_2-adrenoceptor antagonist atipamezole
830 (ATIP, 10 μM), β_1-adrenoceptor antagonist atenolol (ATE, 10 μM), β_2-adrenoceptor
831 antagonist ICI118551 (ICI, 1 μM), and β_3-adrenoceptor antagonist SR59230A (SR, 1 μM)
832 for 3 h. Scale bars = 100 μm. (B, D, F, H, J) The percentage of cells with process formation.
833 More than 200 cells in three random fields were counted. n.s.: not significant (B, unpaired
834 Student's t-test), $^{**}p < 0.01$ (vs. DA alone, D, Dunnett's test), (F, Tukey's t-test), (vs. control,

H and J, Dunnett's test), n = 6. All data are presented as means ± S.E.M.

Figure 6. The effects of dopamine receptor and adrenoceptor agonists on GFAP expression in acute hippocampal slices.

(A) Representative GFAP-stained images of the CA1 areas in acute hippocampal slices treated with dopamine (DA, 10 μM), D1-like receptor full agonist SKF81297 (SKF, 10 μM), and ß-agonist isoproterenol (ISO, 10 μM) for 90 min (Upper left panel: high magnification of the representative astrocyte). Yellow scale bars = 100 μm, green scale bars = 20 μm. (B) The mean grey intensity of GFAP was qualified. The results are expressed as arbitrary units (A.U.). (C-F) The morphology of GFAP-stained astrocytes in the CA1 areas was analyzed using the Fiji-ImageJ Simple Neurite Tracer plugin. The morphological parameters assessed were the total branch length (C), number of branches (D), and average branch length (E); Sholl analysis was also performed (F), which measures the number of intersections at concentric spheres (at 4 μm intervals) originating from the soma (upper right panel). Scale bars = 20 μm. $*p < 0.05$, $**p < 0.01$ vs. control (Dunnett's test), n = 5. All data are presented as means ± S.E.M.

Fig.1

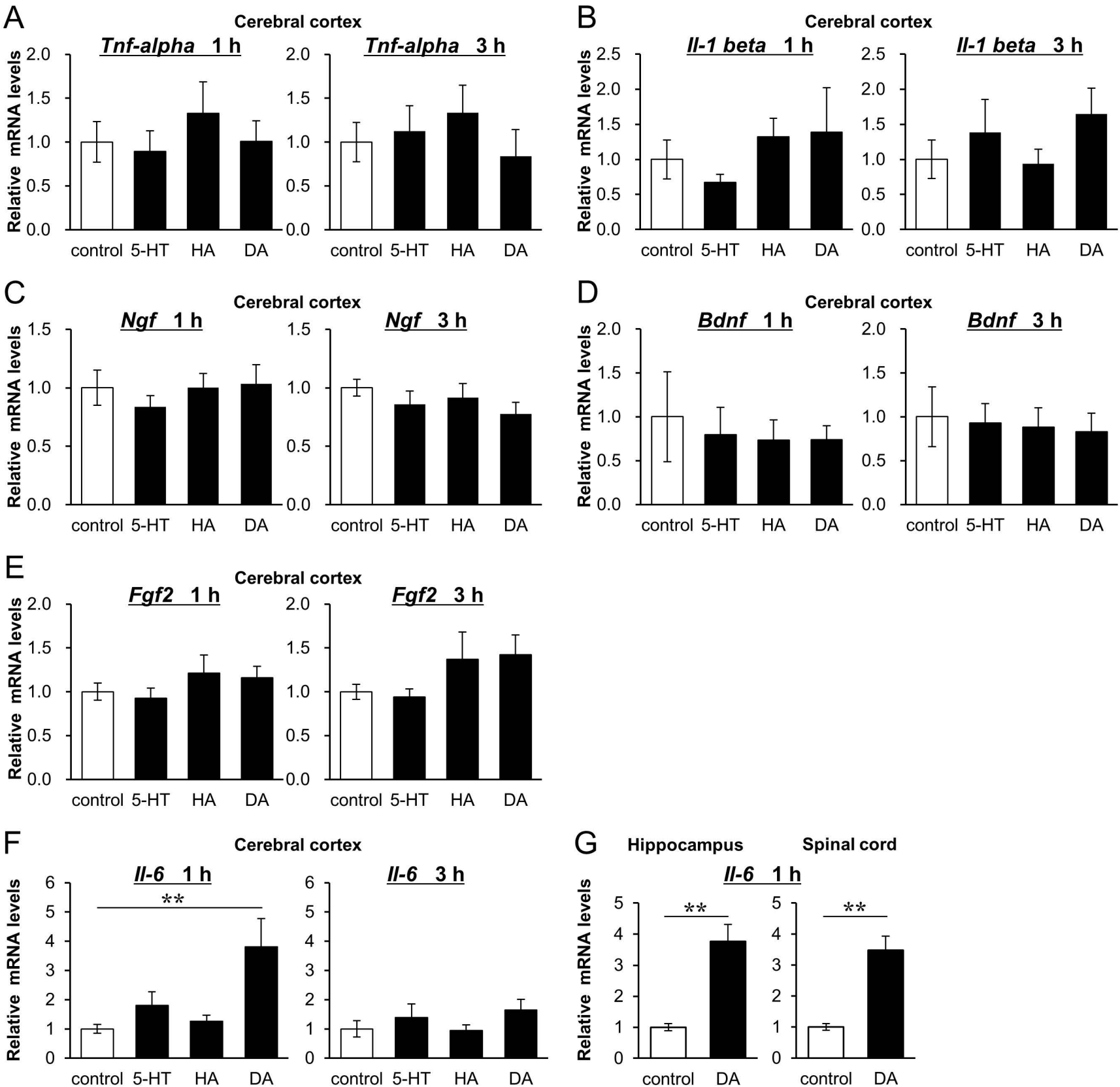
A
Cerebral cortex
Tnf-alpha 1 h
Tnf-alpha 3 h
B
Cerebral cortex
Il-1 beta 1 h
Il-1 beta 3 h
C
Cerebral cortex
Ngf 1 h
Ngf 3 h
D
Cerebral cortex
Bdnf 1 h
Bdnf 3 h
E
Cerebral cortex
Fgf2 1 h
Fgf2 3 h
F
Cerebral cortex
Il-6 1 h
Il-6 3 h
**
G
Hippocampus
Spinal cord
Il-6 1 h
**
**
Relative mRNA levels
control
5-HT
HA
DA

Fig.2

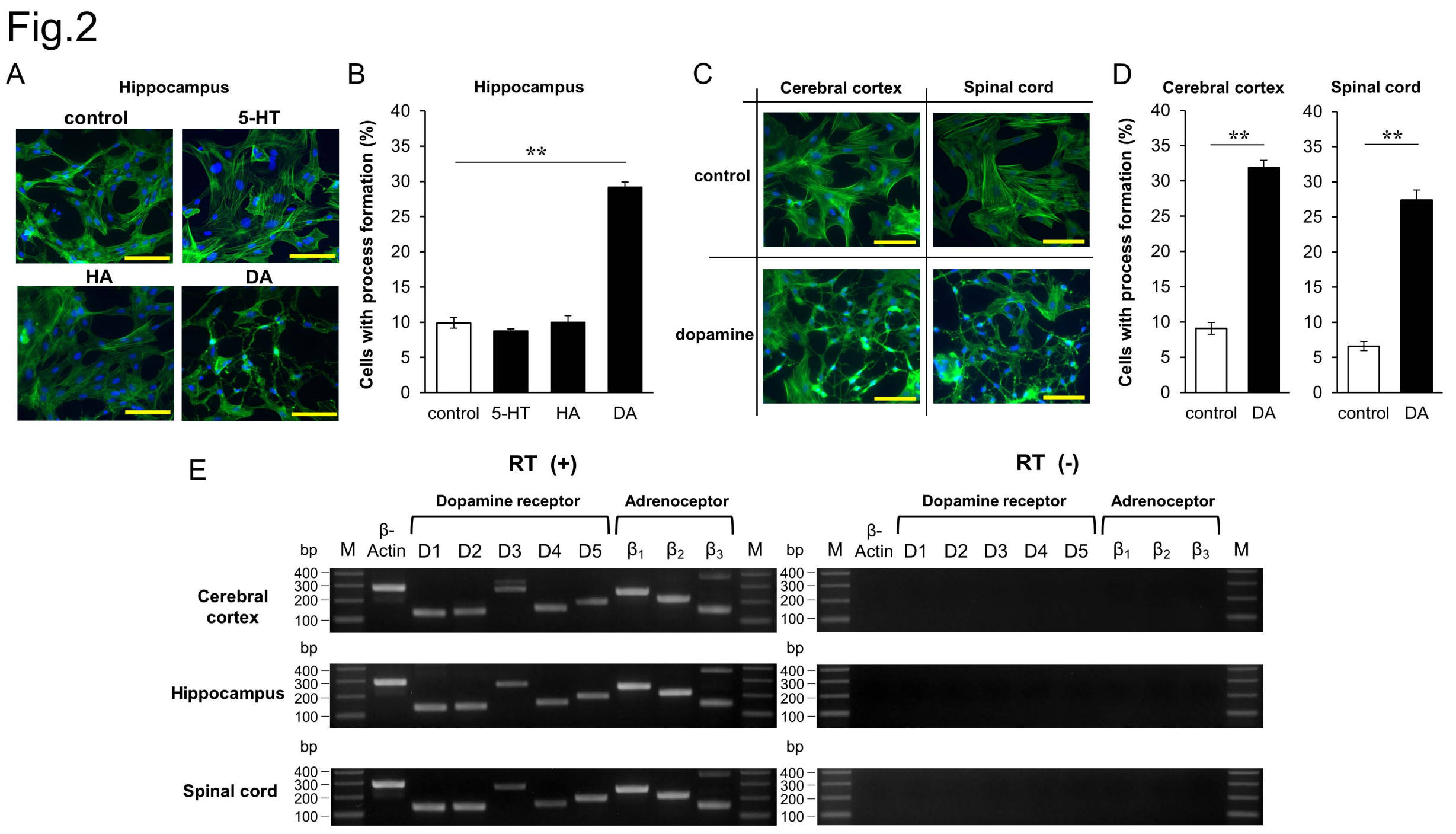
A
Hippocampus
control
5-HT
HA
DA
B
Hippocampus
Cells with process formation (%)
**
control
5-HT
HA
DA
C
Cerebral cortex
Spinal cord
control
dopamine
D
Cerebral cortex
Spinal cord
Cells with process formation (%)
**
**
control
DA
control
DA
E
RT (+)
RT (-)
Dopamine receptor
Adrenoceptor
bp
M
β-Actin
D1
D2
D3
D4
D5
β1
β2
β3
M
400
300
200
100
Cerebral cortex
Hippocampus
Spinal cord

Fig.3

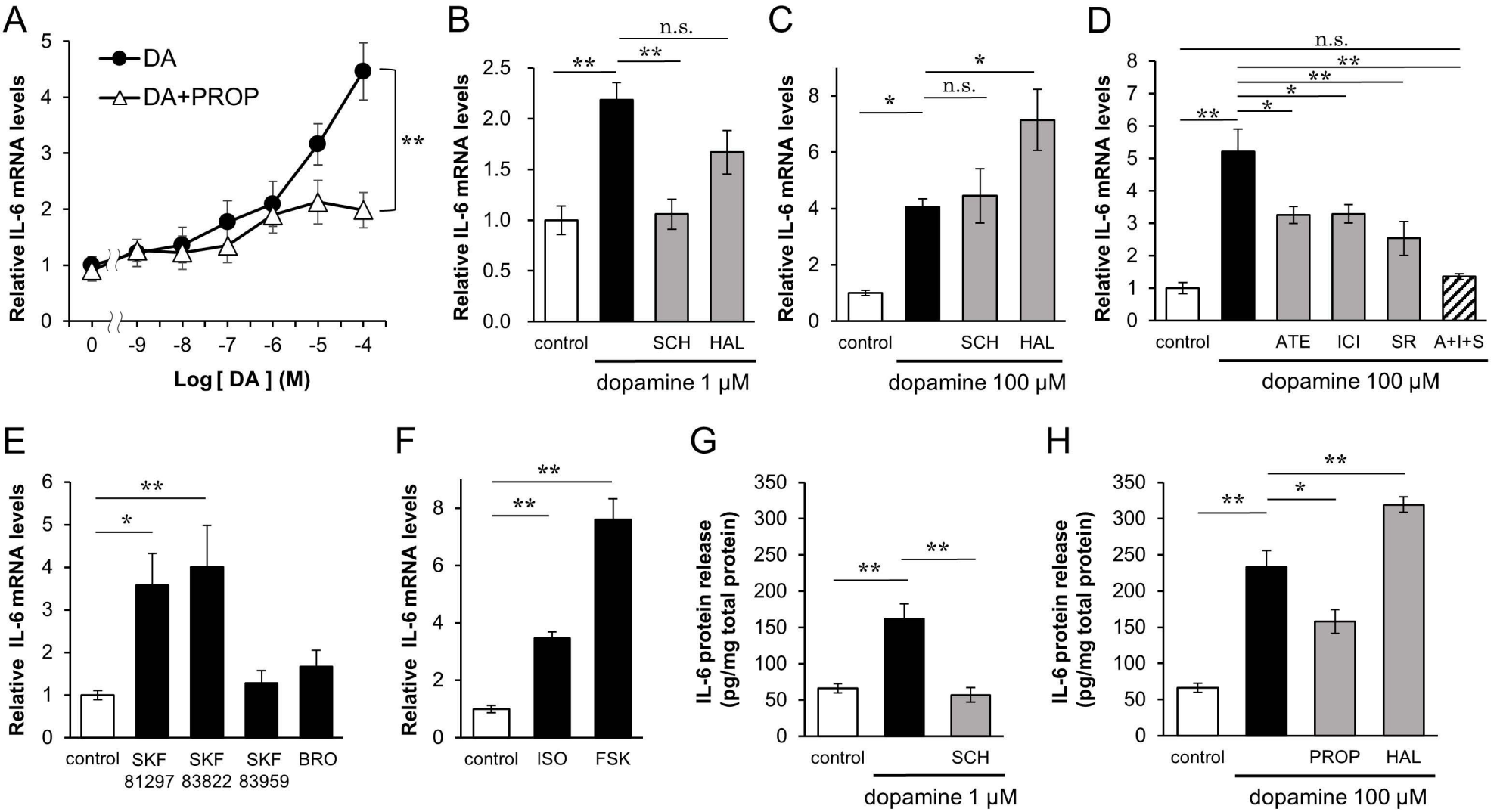
A
DA
DA+PROP
Relative IL-6 mRNA levels
Log [DA] (M)
B
Relative IL-6 mRNA levels
control
SCH
HAL
dopamine 1 μM
C
Relative IL-6 mRNA levels
control
SCH
HAL
dopamine 100 μM
D
Relative IL-6 mRNA levels
control
ATE
ICI
SR
A+I+S
dopamine 100 μM
E
Relative IL-6 mRNA levels
control
SKF 81297
SKF 83822
SKF 83959
BRO
F
Relative IL-6 mRNA levels
control
ISO
FSK
G
IL-6 protein release (pg/mg total protein)
control
SCH
dopamine 1 μM
H
IL-6 protein release (pg/mg total protein)
control
PROP
HAL
dopamine 100 μM

Fig. 4

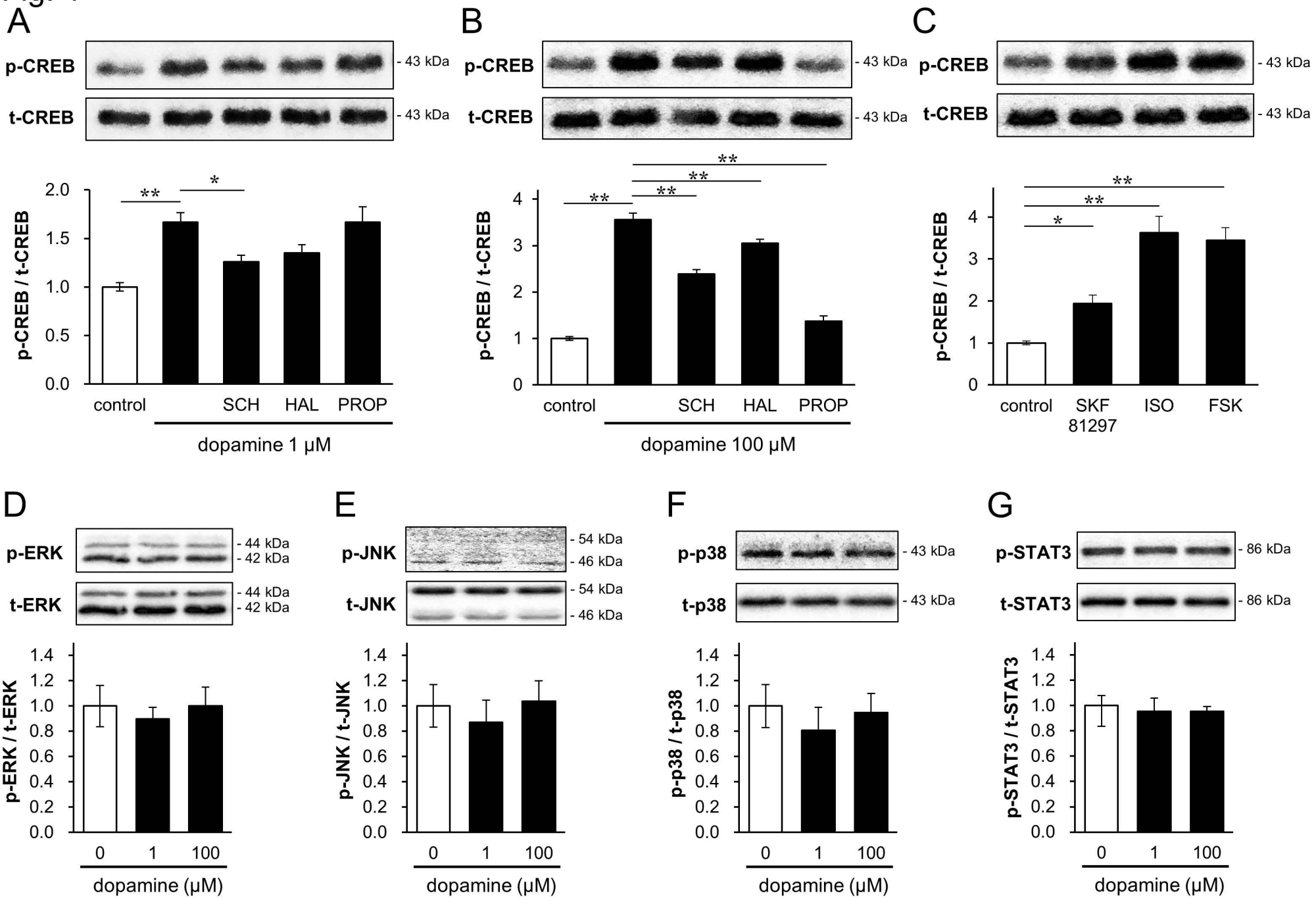
A
p-CREB
t-CREB
- 43 kDa
- 43 kDa
p-CREB / t-CREB
2.0
1.5
1.0
0.5
0.0
**
*
control
SCH
HAL
PROP
dopamine 1 μM
B
p-CREB
t-CREB
- 43 kDa
- 43 kDa
p-CREB / t-CREB
4
3
2
1
0
**
**
**
**
control
SCH
HAL
PROP
dopamine 100 μM
C
p-CREB
t-CREB
- 43 kDa
- 43 kDa
p-CREB / t-CREB
4
3
2
1
0
**
**
*
control
SKF 81297
ISO
FSK
D
p-ERK
t-ERK
- 44 kDa
- 42 kDa
- 44 kDa
- 42 kDa
p-ERK / t-ERK
1.4
1.2
1.0
0.8
0.6
0.4
0.2
0.0
0
1
100
dopamine (μM)
E
p-JNK
t-JNK
- 54 kDa
- 46 kDa
- 54 kDa
- 46 kDa
p-JNK / t-JNK
1.4
1.2
1.0
0.8
0.6
0.4
0.2
0.0
0
1
100
dopamine (μM)
F
p-p38
t-p38
- 43 kDa
- 43 kDa
p-p38 / t-p38
1.4
1.2
1.0
0.8
0.6
0.4
0.2
0.0
0
1
100
dopamine (μM)
G
p-STAT3
t-STAT3
- 86 kDa
- 86 kDa
p-STAT3 / t-STAT3
1.4
1.2
1.0
0.8
0.6
0.4
0.2
0.0
0
1
100
dopamine (μM)

Fig.5

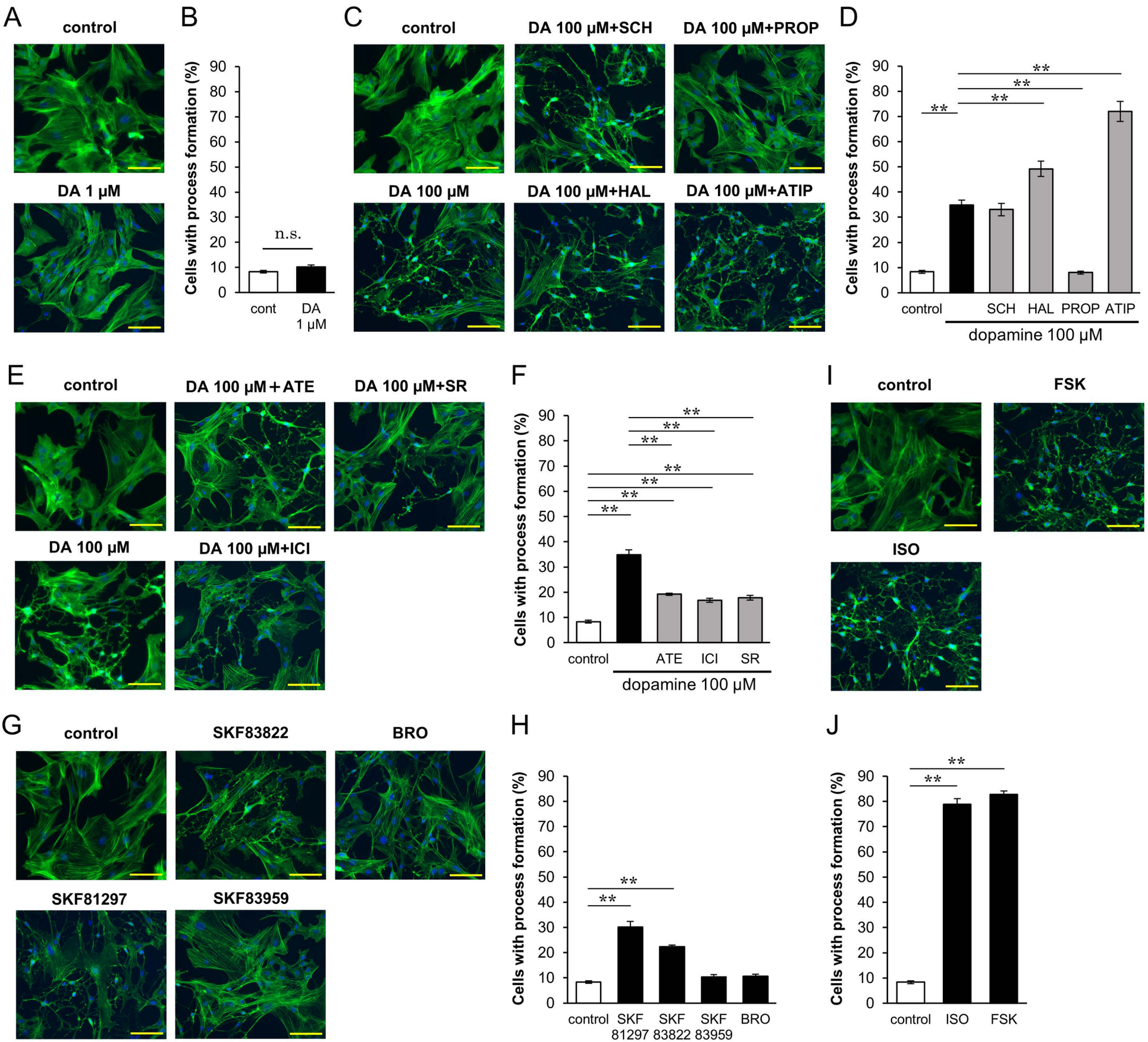
A
control
DA 1 μM
B
Cells with process formation (%)
n.s.
cont
DA 1 μM
C
control
DA 100 μM+SCH
DA 100 μM+PROP
DA 100 μM
DA 100 μM+HAL
DA 100 μM+ATIP
D
Cells with process formation (%)
control
SCH
HAL
PROP
ATIP
dopamine 100 μM
E
control
DA 100 μM＋ATE
DA 100 μM+SR
DA 100 μM
DA 100 μM+ICI
F
Cells with process formation (%)
control
ATE
ICI
SR
dopamine 100 μM
I
control
FSK
ISO
G
control
SKF83822
BRO
SKF81297
SKF83959
H
Cells with process formation (%)
control
SKF 81297
SKF 83822
SKF 83959
BRO
J
Cells with process formation (%)
control
ISO
FSK

Fig.6

A

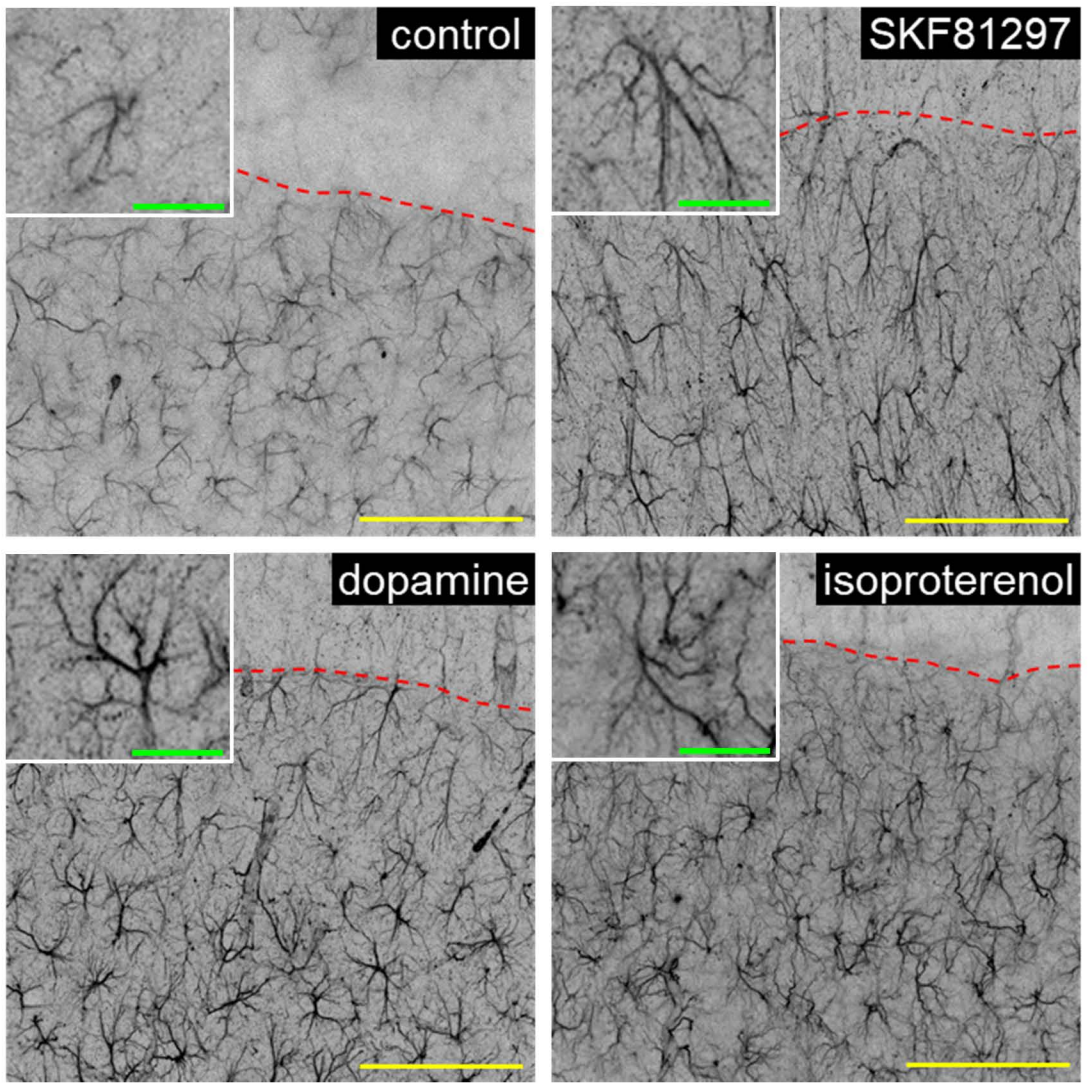
control
SKF81297
dopamine
isoproterenol

B

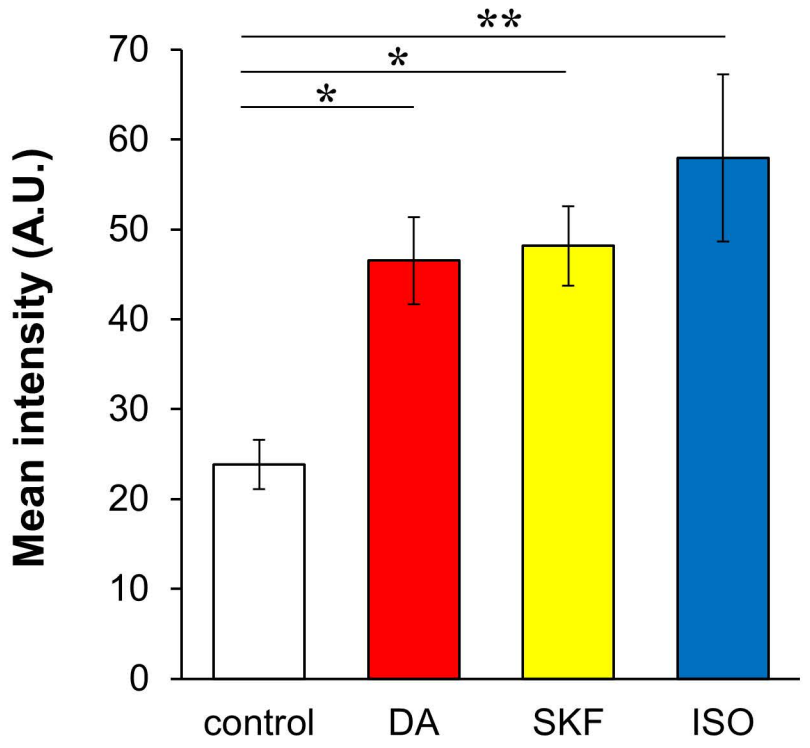
Mean intensity (A.U.)
0
10
20
30
40
50
60
70
*
*
**
control
DA
SKF
ISO

C

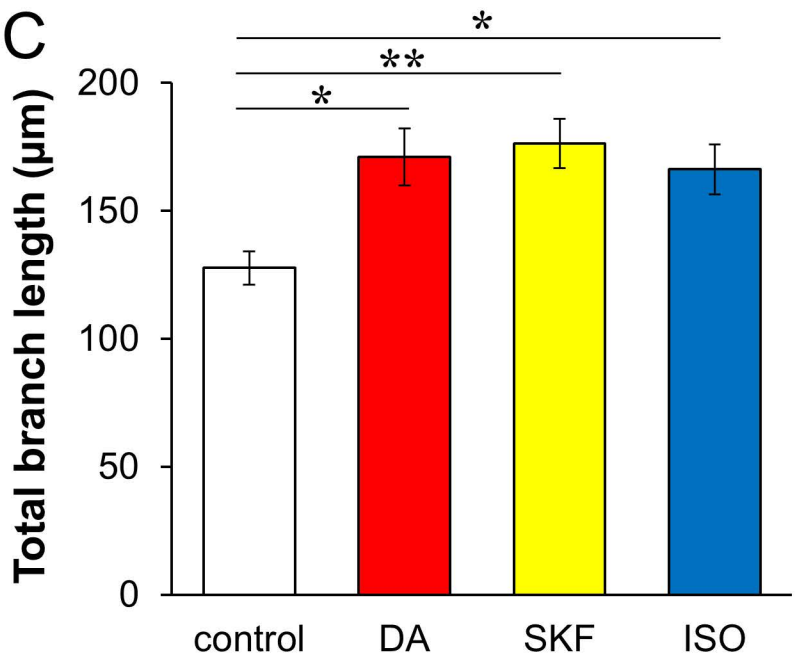
Total branch length (μm)
0
50
100
150
200
*
**
*
control
DA
SKF
ISO

D

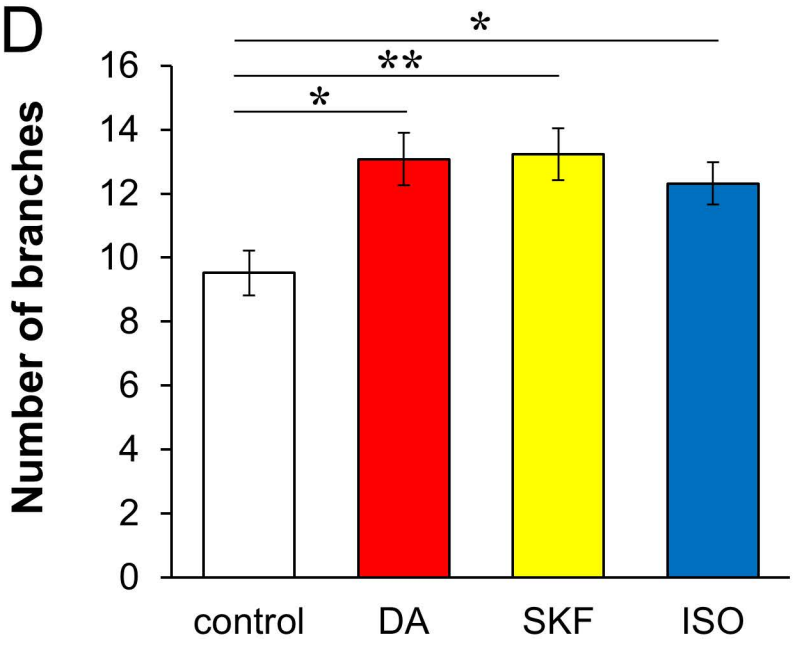
Number of branches
0
2
4
6
8
10
12
14
16
*
**
*
control
DA
SKF
ISO

E

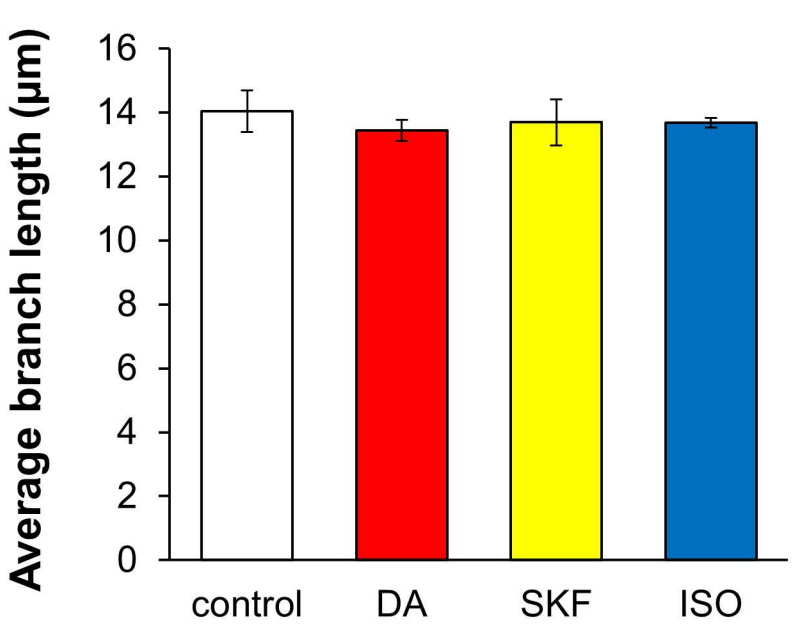
Average branch length (μm)
0
2
4
6
8
10
12
14
16
control
DA
SKF
ISO

F

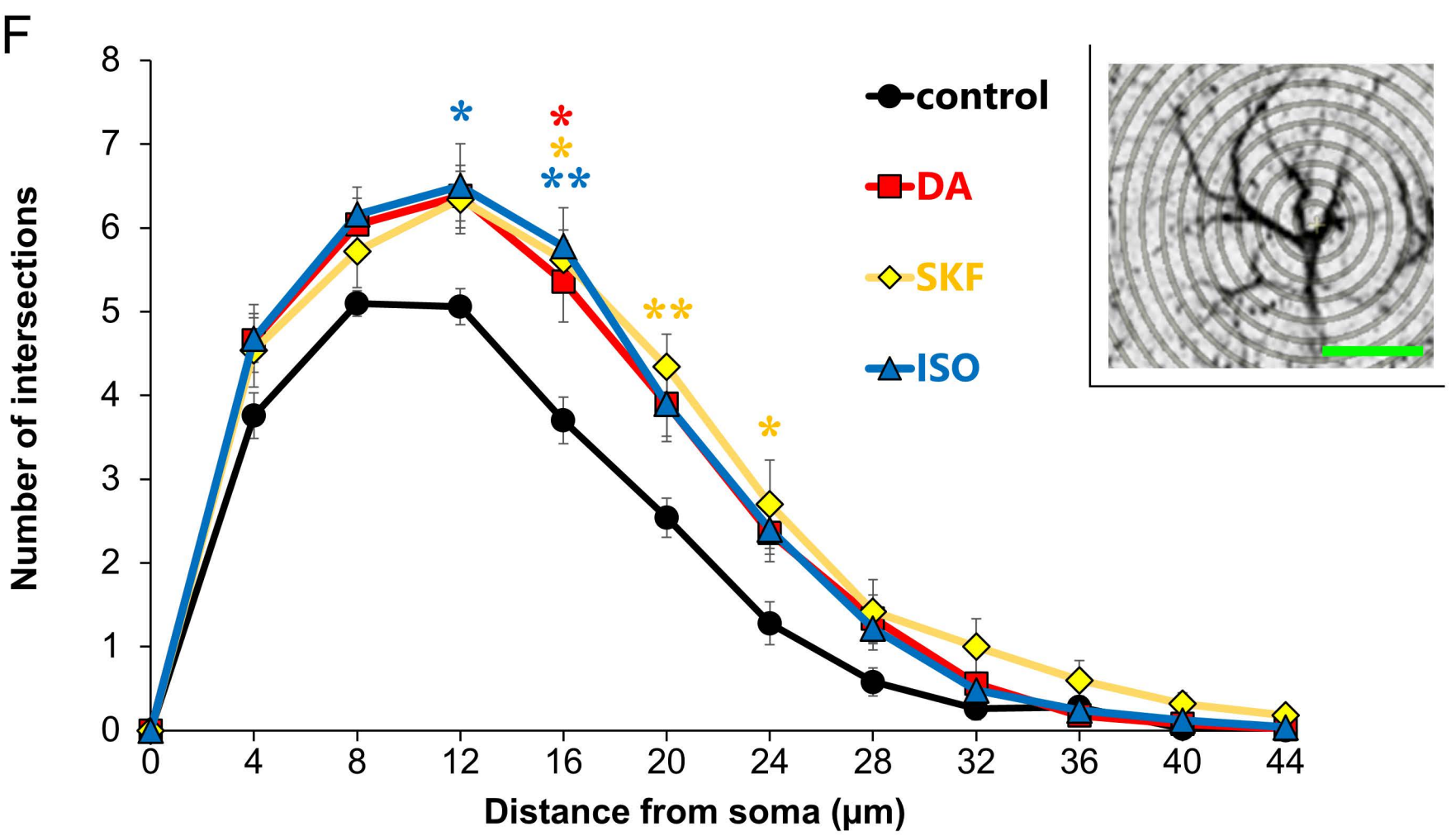
Number of intersections
0
1
2
3
4
5
6
7
8
0
4
8
12
16
20
24
28
32
36
40
44
Distance from soma (μm)
control
DA
SKF
ISO
*
*
*
**
**
*